Biophysical Journal Volume 65 July 1993 469–491



# Solutions for Transients in Arbitrarily Branching Cables: III. Voltage Clamp Problems

Guy Major
University Laboratory of Physiology, Oxford, OX1 3PT, United Kingdom

ABSTRACT Branched cable voltage recording and voltage clamp analytical solutions derived in two previous papers are used to explore practical issues concerning voltage clamp. Single exponentials can be fitted reasonably well to the decay phase of clamped synaptic currents, although they contain many underlying components. The effective time constant depends on the fit interval. The smoothing effects on synaptic clamp currents of dendritic cables and series resistance are explored with a single cylinder + soma model, for inputs with different time courses. "Soma" and "cable" charging currents cannot be separated easily when the soma is much smaller than the dendrites. Subtractive soma capacitance compensation and series resistance compensation are discussed. In a hippocampal CA1 pyramidal neurone model, voltage control at most dendritic sites is extremely poor. Parameter dependencies are illustrated. The effects of series resistance compound those of dendritic cables and depend on the "effective capacitance" of the cell. Plausible combinations of parameters can cause order-of-magnitude distortions to clamp current waveform measures of simulated Schaeffer collateral inputs. These voltage clamp problems are unlikely to be solved by the use of switch clamp methods.

## INTRODUCTION

Analytical solutions for voltage transients in branched cable structures have been presented in Paper I (1) and Paper II (2) of this series. In this paper, the solutions are used to explore some practical problems of space clamp and imperfect voltage clamp. A number of important biological points will be made using two example models: (i) a single cylinder + soma model based on the "basal" half of the layer III cortical pyramidal cell from Paper I, and (ii) the hippocampal CA1 pyramidal cell from Paper I. As in Paper II, two basic voltage clamp scenarios are considered: Case I, synaptic inputs and clamp to zero; and Case II, voltage commands in the absence of synaptic inputs.

The simple geometry of Example 1 will be used to illustrate general points first, before more specific details are considered using the complex geometry of Example 2. Building on the examples in Paper II, further explorations are carried out of: (*a*) the effects of dendritic cables and series resistance on the rise times, peak currents and apparent decay time constants of synaptic clamp currents, (*b*) some results presented recently by Jackson (3), (*c*) the degree of voltage clamp control of subsynaptic voltage swings, (*d*) parameter dependence, and (*e*) propagation of voltage commands down dendritic trees.

The examples are intended primarily to be illustrative, and the explorations are by no means exhaustive. Nevertheless some of the conclusions are likely to be robust, in particular the demonstrations of the inadequacy of voltage clamp for many purposes. For Lists of Symbols, see Papers I and II.

*Received for publication 22 October 1992 and in final form 26 February 1993.*

Address reprint requests to Guy Major at the University Laboratory of Physiology, Parks Rd., Oxford, OX1 3PT, United Kingdom.



0006-3495/93/07/469/23 $2.00

## EXAMPLE 1: SINGLE CYLINDER + SOMA MODEL

Two different aspects of voltage clamp, *a* and *b* above, are investigated in this section, using a single cylinder + soma model.

### The model

The model has the following "raw" morphological and electrical parameters: length $l = 1000$ μm, diameter $d = 10$ μm, soma diameter $d_s = 20$ μm, specific membrane capacitance $C_m = 1$ μFcm$^{-2}$, specific membrane resistance $R_m = 50{,}000$ Ωcm$^2$, cytoplasmic resistivity $R_i = 250$ Ωcm, $g_{shunt} = 0$ nS. With these parameters, the electrotonic length $L = 0.4472$, the soma membrane resistance $R_{sm} = 3.98$ GΩ and the soma capacitance $c_s = 12.57$ pF. The dimensions of the cylinder are the same as those of the "basal" part (i.e., basal + apical oblique dendrites collapsed together) of the two-cylinder + soma model used in Papers I and II (based on a typical rat layer III visual cortical pyramidal cell). The electrical parameters are also well within the biological range of interest (e.g., Refs. 4 and 5).

### Case I: Distortion of synaptic currents by the dendritic cable and series resistance

Both dendritic cables and series resistance can slow and attenuate synaptic currents measured using voltage clamp (e.g., Paper II, Example 2). Rall and Segev (6) and Johnston and Brown (7) concluded that space clamp problems become worse the faster the input time course and that it is therefore important to consider the *frequency-dependent electrical geometry* of the cell as well as the steady-state electrotonic distance of the input site from the clamp point (see also Ref. 8). It is important to re-emphasize these conclusions given mounting evidence that some synaptic conductances may be extremely rapid. Rise times of the order of a few hundred microseconds have been reported (e.g., Refs. 9–15).

*Waveform measures*

A number of waveform measures are commonly used to characterize experimental synaptic clamp currents, for example: peak current, rise time (20–80% or 10–90%), half-width, decay time constant, and half decay time. In general, 20–80% rise times are about 2/3 as long as 10–90% rise times and are probably easier to measure when the waveforms are noisy. Examples of both are given below.

The clamp current waveforms produced by the analytical solution contain a number of exponential components in their decay phases, particularly when the neuronal geometry is complex (e.g., Paper II, Table 2). Included in these are components with time constants associated with the inputs (see Paper I, Responses to Other Inputs section). Despite this, when only one receptor type is activated, the decay phases of both experimental and simulated synaptic clamp currents are often reasonably well fitted by single exponentials (e.g., Refs. 15–18, Ref. 5 (Chapters 5 and 6); also see next section).

Spruston et al. (8), by contrast, found that single exponentials are often inadequate and prefer to use half decay times instead. Decisions about the acceptability of single exponential fits are very dependent on the criteria used. The presence of noise in experimental traces may obscure the presence of multiple time constants. Fits that appear acceptable using a linear voltage axis are often revealed to be inadequate when a logarithmic voltage axis is used: see the discussion on "slow bends" in the Paper I, which applies equally well to clamp currents. Apparent time constants slower than $\tau_0$ can result when fitting starts too soon after the peak, particularly in the case of distal inputs. These caveats apply equally well to compartmental model simulations using synaptic *conductances* as opposed to currents, particularly when the conductance is relatively small compared with the input conductance of the cell, and when it is brief compared with $\tau_0$.

Few studies appear to use statistical criteria in the assessment of fits, but see Refs. 5 and 19 for discussions of "fit standard deviations" (fit S.D.s), defined below, and "goodness-of-fit" (G.O.F.) scores between target and fit waveforms; also see Ref. 5 for a method based on confidence intervals around waveforms. Many studies do not specify the fit intervals used, or whether the time constants vary significantly with changes in interval.

Using the analytical solution waveform generator programs, single exponential currents with total charge 1 pC and various decay time constants $\tau_{sy}$ were injected into the single cylinder + soma model at various locations. The soma was clamped to zero (rest) via various series resistances $R_{ser}$, and the clamp currents were recorded. Peak currents and 20–80% rise times ($t_{2080}$) were measured.

Given that experimenters do regularly quote decay time constants, some compromises are necessary in order to gain modelling insights into this waveform measure. *Apparent* (effective) decay time constants $\tau_{eff}$ were estimated following the standardized procedure in Ref. 15: each clamp current waveform was fitted with a single exponential between $t_{peak}$ + 0.7 and $t_{peak}$ + 20 ms, using peeling (20), and two fitting programs, one based on the Levenberg-Marquardt and the other on the simplex algorithm (Ref. 21, Chapter 10). These fit intervals are somewhat arbitrary, but seemed to work reasonably well for this model, the CA1 pyramidal cell model described in the next section, and for a CA3 pyramidal cell model (Refs. 5 (Chapter 6) and 15). Obviously the intervals would have to be adjusted in cases where the membrane time constants were much slower or faster than the 50 ms used here. In the future, to allow easier comparison between studies, it may be helpful if experimenters and modellers estimate $\tau_{7525}$ (the effective time constant over the interval $t_{75}$ to $t_{25}$) or $t_{7327}$ ($t_{27} - t_{73}$), as discussed in Paper II. The warnings in Paper I are repeated here: the time constants obtained can be very sensitive to the exact interval chosen!

The fit S.D. is calculated as

$$\text{S.D.} = \left( \sum_{i=i1}^{i2} (D_i - F_i)^2 / n \right)^{1/2}, \qquad (1)$$

where $i1$ and $i2$ are the indices of the first and last points in the fit interval, $n = i2 - i1 + 1$, $D_i$ is the $i$th data value, and $F_i$ is the value of the $i$th point in the fit waveform. The fit with the smallest S.D. from the target was selected (in most cases all three methods gave very similar results). *Here*, fits with an S.D. $> 0.003$ appeared unacceptable by eye, and were rejected. Fits with an S.D. $< 0.0003$ appeared very good by eye. It must be emphasized that these criteria apply *only* to this situation: changes in the input or the model, or the addition of noise, could make a quantitative difference. For the current waveforms produced by the single cylinder + soma model, most of the optimal single exponential S.D. values were around 0.001–0.003, i.e., the fits were far from perfect, but were plausible when inspected using a linear current axis. When the current was inverted and a logarithmic current axis was used, however, it was obvious in many cases (particularly for the more distal inputs) that the interval spanned an upwardly convex portion of the waveform: the apparent time constant was slower than $\tau_0$. Many of the more proximal inputs showed the opposite behavior: the apparent time constant was faster than $\tau_0$, because the fit interval occurred during an upwardly concave part of the waveform, or slow bend (see Paper I). In all cases $\tau_{eff}$ was slower than $\tau_{sy}$.

These points are illustrated in Fig. 1. The top two panels show waveforms plotted with linear current axes, the lower two show the same transients using logarithmic current axes. In the left-hand panels, a single exponential current with a decay time constant $\tau_{sy}$ of 2 ms and a total charge $Q$ of 1 pC is injected into the model at one of four locations (the soma, and $z$ = 100, 200, and 1000 $\mu$m). The soma is perfectly clamped to zero. The resulting clamp current waveforms in Fig. 1 *A* (*dotted lines*) demonstrate the filtering effect of the dendritic cable: the clamp current becomes progressively more smoothed, and its peak becomes more attenuated as the input site is moved away from the soma. The solid lines are the optimal single exponential fits to each response: although the fits are not perfect, it is easy to imagine that with the

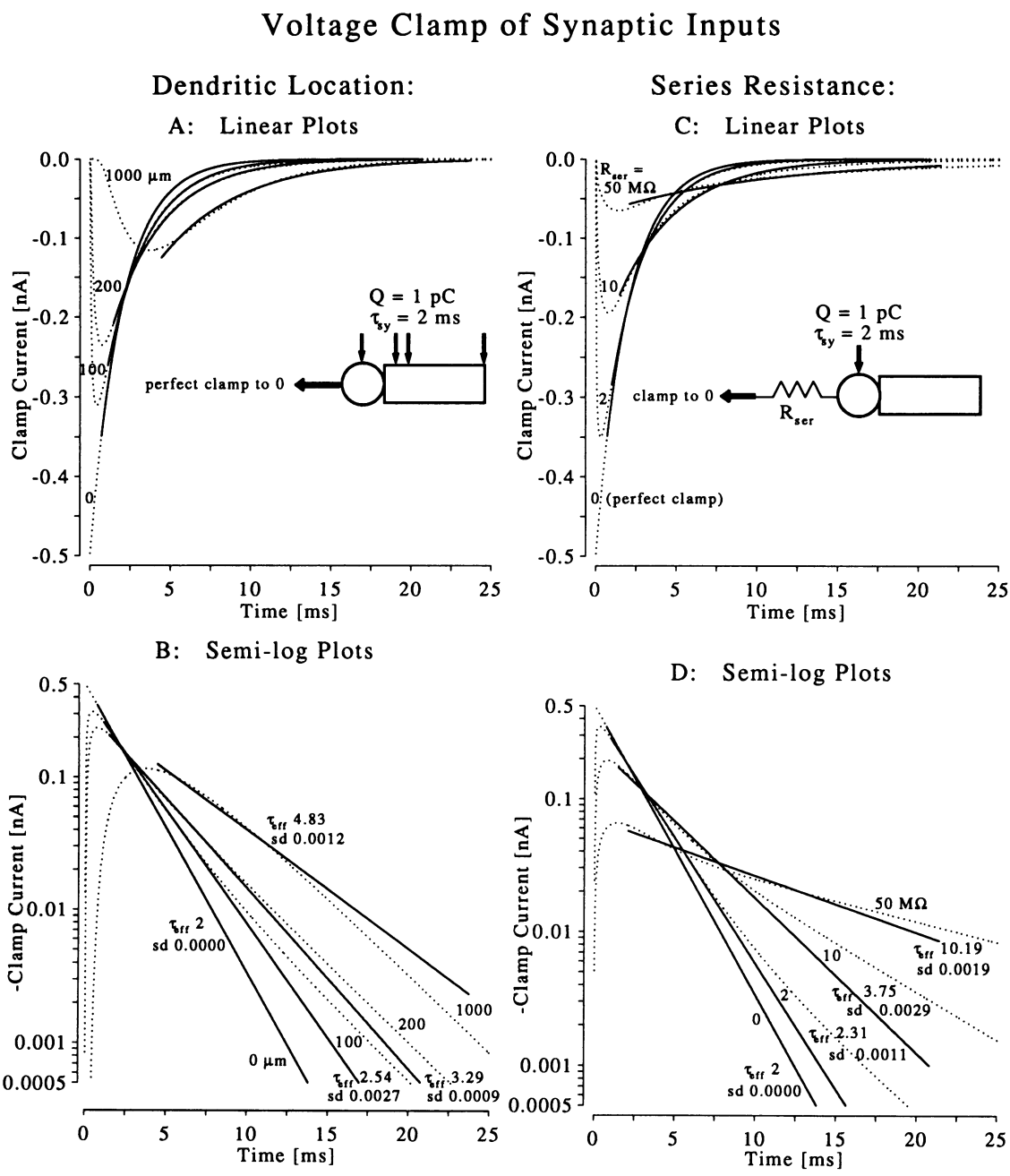


FIGURE 1 Single cylinder + soma model, $l$ = 1000, $d$ = 10, $d_s$ = 20 µm, $C_m$ = 1 µFcm$^{-2}$, $R_m$ = 50,000 Ωcm$^2$, $R_i$ = 250 Ωcm, $g_{shunt}$ = 0. Synaptic clamp currents in response to single exponential inputs, with decay time constant $\tau_{sy}$ = 2 ms and total charge $Q$ = 1 pC. Top panels, linear current axis; bottom panels, −1× current plotted with logarithmic current axis. Dotted lines, model responses; solid lines, optimal fits, plotted only for duration of fit interval or until current < 0.5 pA. In lower panels, fit S.D. values (sd) and effective time constants $\tau_{eff}$ (in milliseconds) are written alongside the corresponding waveforms. (*A* and *B*) effect of distance from soma $z$: four input sites at 0, 100, 200, and 1000 µm from soma. Soma perfectly clamped to zero. (*C* and *D*) effects of series resistance ($R_{ser}$) on the somatic input. Clamp to zero via four values of $R_{ser}$ (0, 2, 10, and 50 MΩ), indicated alongside relevant response. Increasing both $z$ and series resistance causes smoothing of the responses, decreasing the peak current and increasing the rise time and $\tau_{eff}$.

addition of some noise they would appear acceptable. In Fig. 1 *B*, the use of a logarithmic current axis gives a worse impression of the fits, but it is important to remember that any noise would also be more evident at the tails of the plots: the graphs span 3 log units (a factor of 1000). The fit S.D. values are written alongside each waveform, together with the apparent time constant $\tau_{eff}$. It can be seen that $\tau_{eff}$ increases as the injection site is moved away from the soma.

In the right-hand panels of Fig. 1 are shown the effects of four different series resistances upon the somatic input's clamp current. It can be seen that increasing $R_{ser}$ also smooths the waveforms and attenuates the peaks (*C*, *dotted lines*). The single exponential fits (*solid lines*) also appear adequate, although when re-examined with a semi-log plot (*D*), it is obvious that more than one exponential component makes a significant contribution during the fit interval (except for the

perfect clamp case). The imperfect clamp responses demonstrate clear slow bends analogous to those seen in Paper I, Example 2. Again, $\tau_{eff}$ grows with $R_{ser}$.

Compared with the single cylinder + soma model, the more complicated geometry of the CA1 pyramidal all in the next example produced a larger number of exponential components making significant contributions to a given response waveform over the fit interval. The larger number of time constants produced smoother and slower changes in the overall effective time constant, allowing better single exponential fits. This phenomenon, coupled with noise, may explain why single exponential fits of experimental "clamped" synaptic currents (resulting from activation of one receptor type) are so frequently found to be acceptable. It is still urged, however, that these time constants should be termed "apparent" or "effective" time constants, because of the large number of "real" time constants underlying them.

### *Systematic explorations of synaptic location, $R_{ser}$ and $\tau_{sy}$*

The results of many single cylinder + soma model simulations are summarized in Figs. 2 and 3. These figures are intended to convey the effects of varying three model parameters: input location $z$, series resistance $R_{ser}$, and synaptic time constant $\tau_{sy}$. The morphology and electrical parameters are held constant throughout.

In Fig. 2, $\tau_{sy}$ is fixed at 2 ms. Instead of three-dimensional plots of each waveform measure versus $R_{ser}$ and $z$, the same data are plotted twice, once versus $z$ for several values of $R_{ser}$ (*A–C* on the left) and again versus $R_{ser}$ for several values of $z$ (*D–F* on the right).

In Fig. 2 *A* it can be seen that the peak current "efficacy," i.e., the peak *measured* current (peak $i_{clamp}$) divided by the peak *actual* input current (peak $i_{syn}$) falls off with $z$. Most of the decrease is over the proximal part of the dendrite. There is little change in efficacy over the distal half of the cylinder (a so-called "end effect"). Increasing the series resistance decreases the efficacy at all locations, but also reduces the proximal-to-distal fall-off. The same data is replotted against $R_{ser}$ in Fig. 2 *D*; increasing $R_{ser}$ strongly filters the peakier proximal inputs but has less effect on the more distal inputs which are already appreciably smoothed by the cable.

The 20–80% rise times increase with $z$, at first approximately linearly, then more steeply, and finally, near the distal end (800–1000 $\mu$m), they level off (Fig. 2, *B* and *E*). The "correct" value of 0 ms (for an instantly rising single exponential input) is shown by the arrow. Increasing series resistance causes further slowing. The effect is slightly more pronounced for the more distal inputs and diminishes with increasing $R_{ser}$.

Similarly, effective decay time constants appear to increase approximately linearly over the initial part of the cable, and then level off for most of the distal half (Fig. 2 *C*). The $\tau_{eff}$ values increase approximately linearly with $R_{ser}$ up to about 50 M$\Omega$ (Fig. 2 *F*). The rate of increase is slightly greater for distal than for proximal inputs (the lines diverge slightly). These straight line relationships are discussed in Paper II (Parameter Dependence of Imperfect Clamp Impulse Response section). The correct synaptic current time constant of 2 ms is indicated by an arrow.

The effects on the peak current of the series resistance and the distance $z$ of the input from the soma are less than additive. To a good approximation however, the effects of $z$ and $R_{ser}$ are additive for the $t_{2080}$ and $\tau_{eff}$ values. An increase in $R_{ser}$ produces a nearly constant vertical offset in the plots against $z$ (Fig. 2, *B* and *C*). The magnitude of the offset decreases for larger $R_{ser}$ values. Likewise, increases in $z$ produce nearly constant vertical offsets in the plots against $R_{ser}$ (Fig. 2, *E* and *F*). The additional changes diminish as $z$ nears 1000 $\mu$m.

The effects of changing the input current decay time constant are explored in Fig. 3. A range of $\tau_{sy}$ values are tested, from 0 (i.e., an impulse or $\delta$ function) to 10 ms. In the left-hand panels, the waveform measures are plotted against location for a model with $R_{ser} = 0$, for a number of different $\tau_{sy}$ values. The right-hand panels illustrate the combined effects of $z$, $\tau_{sy}$, and $R_{ser}$ on the $\tau_{eff}$ values.

As shown in a number of studies (e.g., Refs. 6–8), the fall-off in peak current efficacy becomes steeper as the input becomes faster (Fig. 3 *A*). All the plots show end effects. The decrement with $z$ for a constant current input is also shown for reference. Because of the reciprocity relations discussed in Paper II, these plots are the same as the decrement with $x$, the recording position, of equivalent voltage commands at the clamp point (also see Ref. 6). The clamp current in response to a constant input at the distal end of the cable ($L = 0.447$) is about 91% of the actual input current. With $\tau_{sy} = 1$ ms, however, the peak clamp current is only 14% of the peak input current, underlining how misleading electrotonic distance alone is as a guide to the effects of cables on transients.

Fig. 3 *B* shows that rise times increase with $\tau_{sy}$, and this increase is more pronounced for the more distal inputs. End effects like those in Fig. 2 *B* can also be seen.

In Fig. 3 *C* it can be seen that effective decay time constants increase with $\tau_{sy}$. The different lines are separated by almost constant offsets. The end effects become more pronounced for slower inputs. Replotting the same data against $\tau_{sy}$ (Fig. 3 *D*), shows that (except for very fast distal inputs), $\tau_{eff}$ is approximately linearly dependent on $\tau_{sy}$. A number of points on these two plots are missing: the corresponding fits appeared unacceptable and had S.D. values $> 0.003$. The fractional errors in $\tau_{eff}$ are smaller for the slower inputs: for example, for the tip inputs ($z = 1000$), $\tau_{eff}/\tau_{sy}$ is 4.08 when $\tau_{sy} = 1$ ms, but only 1.3 when $\tau_{sy} = 10$ ms.

The additional influence of series resistance is illustrated in Fig. 3 *E*. The lines for the soma and tip ($z = 1000$) inputs from the previous panel ($R_{ser} = 0$) are shown, together with equivalent data from models with $R_{ser} = 20$ and 50 M$\Omega$. Increasing series resistance increases both the initial offset and the rate of increase of $\tau_{eff}$ with $\tau_{sy}$. The rate of increase is steepened more for the somatic than for the tip input. For

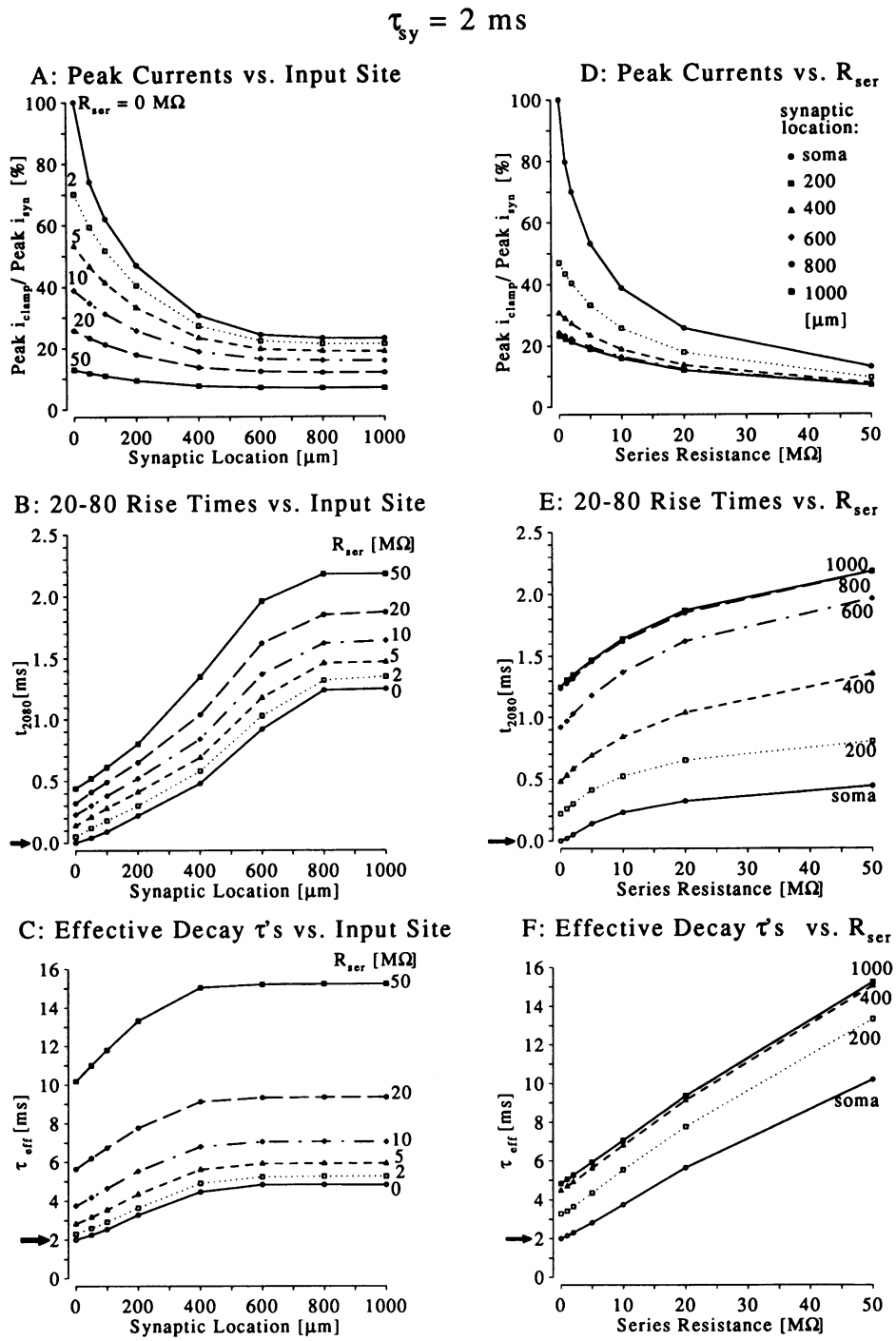


FIGURE 2 Single cylinder + soma model: clamp current waveform measures from responses to a single exponential input with a decay time constant $\tau_{sy}$ of 2 ms. Other parameters as before. "Correct" values (i.e., those of synaptic input itself) are indicated by arrows. Panels on left (*A–C*), measures versus synaptic location *z*. Different lines are labeled with the $R_{ser}$ used. Panels on right (*D–F*), measures versus $R_{ser}$. Different lines are marked with the input location used (*symbols* given in key in D). (*A* and *D*) peak current efficacy, i.e., measured peak clamp current ($i_{clamp}$) ÷ real peak synaptic current ($i_{syn}$). (*B* and *E*) 20–80% rise times ($t_{2080}$ values). (*C* and *F*) effective decay time constants $\tau_{eff}$: optimal fits from peak + 0.7 ms to peak + 20 ms.

$R_{ser} > 0$, the somatic and tip effective decay time constants converge for the slower inputs. This convergence is more rapid the higher $R_{ser}$, because filtering by the series resistance begins to dominate filtering by the dendritic cable. The influence of $\tau_{sy}$ on the increases in $\tau_{eff}$ with series resistance are shown in Fig. 3 *F*. The proximal-distal differences shrink with large $R_{ser}$ and $\tau_{sy}$ (since the cable is relatively less important). The initial intercepts increase with $\tau_{sy}$, as would be predicted from Fig. 3 *D*. The rates of increase with $R_{ser}$ also steepen as $\tau_{sy}$ grows. The fractional errors in $\tau_{eff}$, however, are smaller for the slower inputs. For example, for the somatic input and $R_{ser}$ = 50 MΩ, $\tau_{eff}/\tau_{sy}$ is 5.1 when $\tau_{sy}$ = 2 ms, and only 2.9 when $\tau_{sy}$ = 10 ms.

In summary, this simple model shows that serious errors in all three clamp current waveform measures can occur because of filtering by the dendritic cable and by the series resistance. For a single exponential input, the fractional errors in peak measured current and apparent synaptic decay time constant $\tau_{eff}$ become smaller as the input time constant $\tau_{sy}$ is slowed. The $\tau_{eff}$ values are approximately linearly de-

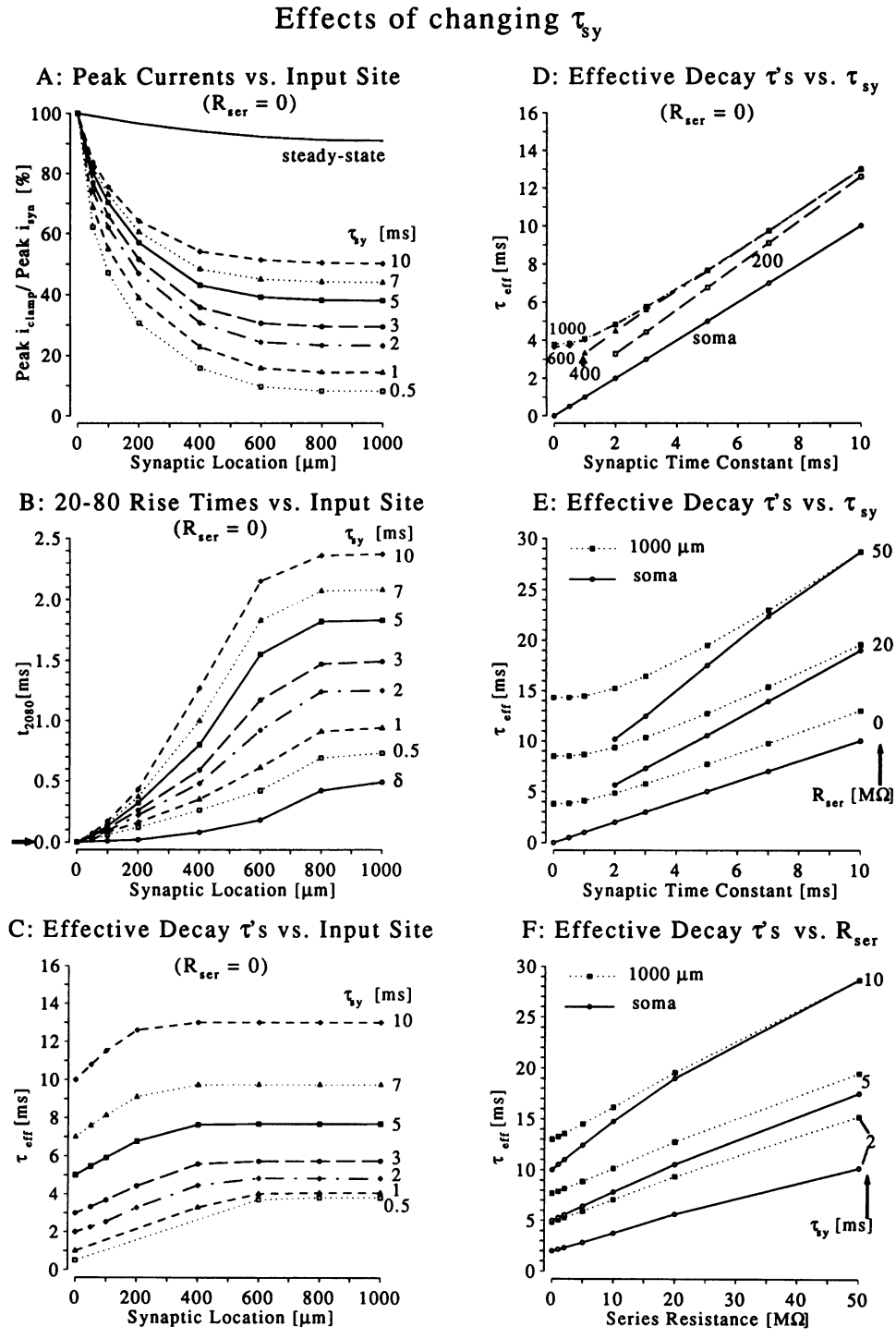


FIGURE 3 Single cylinder + soma model: clamp current waveform measures from responses to single exponential inputs with different decay time constants $\tau_{sy}$. Other parameters as before. Panels on left (*A–C*), measures versus synaptic location $z$, $R_{ser}$ = 0. Different lines are labeled with the $\tau_{sy}$ used. δ = instantaneous charge impulse (i.e., $\tau_{sy}$ = 0). (*C–F*), effective decay time constants $\tau_{eff}$: optimal single exponential fits from peak + 0.7 ms to peak + 20 ms. Points corresponding to unacceptable fits are omitted in *C–E*. (*A*) peak current efficacy, i.e., measured peak clamp current ($i_{clamp}$) ÷ real peak synaptic current ($i_{syn}$). D.C. steady-state response also shown. (*B*), 20–80% rise times versus location. (*C*), $\tau_{eff}$ values versus location. (*D*) $\tau_{eff}$ values versus $\tau_{sy}$, $R_{ser}$ = 0. Lines labeled with synaptic locations. Note that the lines for $z$ = 600 to 1000 μm superimpose almost exactly, and the 400 μm line converges with them when $\tau_{sy}$ is large. (*E*) $\tau_{eff}$ values versus $\tau_{sy}$, for three values of $R_{ser}$ (indicated on right). Data for two input locations, soma and tip (1000 μm), are plotted at each $R_{ser}$. The lower pair of lines correspond to the outermost lines in *D*. (*F*) $\tau_{eff}$ values versus $R_{ser}$, for three values of $\tau_{sy}$ (indicated on right). Data for soma and tip inputs are plotted at each $R_{ser}$.

pendent on both $\tau_{sy}$ and $R_{ser}$, and their dependence on $z$ is roughly linear for proximal inputs, flattening off as the tip is approached.

Although the errors will depend on the precise morphological and electrical parameters of the model, the broad trends illustrated here will hold for a wide range of models. A similar analysis is performed as part of the next example, with additional explorations of the effects of changing the electrical parameters.

## Case II: Voltage steps—exploration of Jackson's results

In a recent paper on cable analysis with the whole cell patch clamp technique (3), Jackson presented an approximate separation of variables solution for the clamp current into a single cylinder + soma model with a voltage step imposed via a series resistance. This study established a number of results of considerable practical importance to experimenters

attempting to voltage clamp neurones. In all cases it was assumed that $R = R_{sm}/R_{ser} > 100$ (i.e., the series resistance was less than 1% of the soma membrane resistance $R_{sm}$). An exploration of these results provides an interesting opportunity to illustrate the single-cylinder + soma special cases of the analytical solutions presented in Paper II, (II.33) and (II.48).

### *Particular results considered*

The results in Ref. 3 included:

1) One waveform component in the solution, with $\alpha = \alpha_R$, has a time constant $\tau_R \approx R_{ser}c_s$, the charging time constant, via the series resistance, of the soma with the dendrites stripped away.

2) The other time constants, associated with "cable charging," should be virtually insensitive to $R_{ser}$. Only $\alpha_R$ (and $\tau_R$) should vary with $R_{ser}$.

3) If the ratio of the two slowest time constants exceeds 9, this is evidence that no equivalent cylinder can account for the observed transient.

4) The amplitude of the $\tau_R$ ("soma charging") term is much larger than the other amplitudes of the other components. The soma charging and cable charging currents can therefore be distinguished on a practical basis.

5) The soma capacitance can be compensated by "balancing out" the "fast" part of the current transient in the "routine" way for amplifiers such as the EPC-7 (List), using the G-series and C-slow dials (or their equivalent). Following this, the clamp current can be "sharpened-up" by means of series resistance compensation.

### *Likely values of $\rho_\infty$*

Jackson noted that his approximations generally become poorer for larger $\rho_\infty = g_\infty/g_{sm}$ (ratio of input conductance of infinitely extended cylinder to soma membrane conductance). Note that his definition of $\rho_\infty$ does not include any somatic shunt $g_{shunt}$. When his solution was tested using a model with a soma that was very large compared to the dendrite ($d_s$ = 20 $\mu$m, $d$ = 1.08 $\mu$m, $l$ = 385.6 $\mu$m, "raw" electrical parameters as in the section titled "The Model" above), the approximation was found to be a good one (not illustrated). However, $\rho_\infty$ for this model was only 2.

In the no-shunt case (i.e., $g_{ser}$ finite but $g_{shunt} = 0$), $\rho_\infty$ can be written

$$\rho_\infty = \frac{d^{3/2}}{2d_s^2}\sqrt{R_m/R_i}. \tag{2}$$

It can be seen that $\rho_\infty$ is the product of two terms, one purely morphological ($d^{3/2}/2d_s^2$), the other purely electrical $\sqrt{R_m/R_i}$). This "root resistivity ratio" or "morphoelectric factor" was introduced in Ref. 22. With a $d^{3/2}$ of 22 $\mu m^{3/2}$, based on the average of the *initial* values for rat visual cortical layer II/III and layer V pyramidal cells (22, Fig. 2), and a $d_s$ of 18.5 $\mu$m (the mean soma (height + width + width)/3 over all three classes of cell in Table I of Ref. 23, $d^{3/2}/2d_s^2 = 32.1$ $m^{-1/2}$. Since, for these cells, $R_m$ is unlikely to be below 10,000 $\Omega cm^2$ and $R_i$ may be as high as 400 $\Omega$cm (see Refs. 4, 5, and 24), the morphoelectric factor is probably larger than 0.5 $m^{1/2}$. When dendritic spines, which account for about half the surface area of the cells, are included using a "folding factor" $F$ (see Paper I, Fig. 2 legend), where

$$F = \frac{\text{area including spines}}{\text{area without spines}} \tag{3}$$

(22), $d^{3/2}$ must be multiplied by another factor of $F^{1/2}$ which is approximately $\sqrt{2}$ here. Thus the minimum value for $\rho_\infty$ is $32.1 \times \sqrt{2} \times 0.5 = 22.7$. A more likely value for the morphoelectric factor is 1.414 $m^{1/2}$ (parameters above: $R_m$ = 50,000 $\Omega cm^2$, $R_i$ = 250 $\Omega$cm; see Ref. 5 for justification) giving a $\rho_\infty$ of 64.2. For comparison, the mean dendritic area (including spines) ÷ soma area over all three classes of pyramidal cell was 31.9 (from figures in Table 2 of Ref. 22).

The single cylinder + soma model introduced in the previous section has a $\rho_\infty$ of 55.9, probably not atypical for cortical pyramidal cells. This figure is an order of magnitude higher than the values tested in Ref. 3. It is interesting to see how well Jackson's assertions perform for this model, which has, arguably, a more "realistic" $\rho_\infty$ than those he considered.

### *Testing results 1–4 with the high $\rho_\infty$ model*

Using the analytical solutions in the previous two papers, and the model described above (The Model section), a 1-mV step command was imposed on the soma via various series resistances, and the time constants and clamp current amplitudes and waveforms were generated. In all cases the waveforms agreed extremely closely with those obtained from equivalent compartmental model simulations. With the parameters specified above, the electrotonic length $L = 0.4472$, the soma membrane resistance $R_{sm} = 3.98$ G$\Omega$, and the soma capacitance $c_s = 12.57$ pF. The discussion in this section is limited to models with $R_{ser} \leq 40$ M$\Omega$ (i.e., $R \geq 100$). It should be noted that Jackson quotes a stricter criterion for his approximations to hold: $R > 121/L^2$, in this case $R > 605$, i.e., $R_{ser} < 6.6$ M$\Omega$.

Selected time constants and amplitudes from the model are plotted against series resistance in Fig. 4. The time constants are shown in Fig. 4 *A*. The hypothetical soma-alone charging time constant $R_{ser}c_s$ is also plotted against $R_{ser}$: it can be seen that, within the range of series resistances on the graph, it crosses the lines for all of the time constants with an index greater than 1. By choosing an appropriate $R_{ser}$, it is possible to obtain an $R_{ser}c_s$ approximately midway between any pair of neighboring time constants with $n > 1$ (e.g., when $R_{ser}$ = 2, 30, and 40 M$\Omega$: see Table 2). This finding weakens Result 1, although $R_{ser}c_s$ is never "far" from one of the $\tau_n$ values.

It can be seen from Fig. 4 *A* that $\tau_0$ increases almost linearly with $R_{ser}$: the solid line is the value of $\tau_0$ predicted by

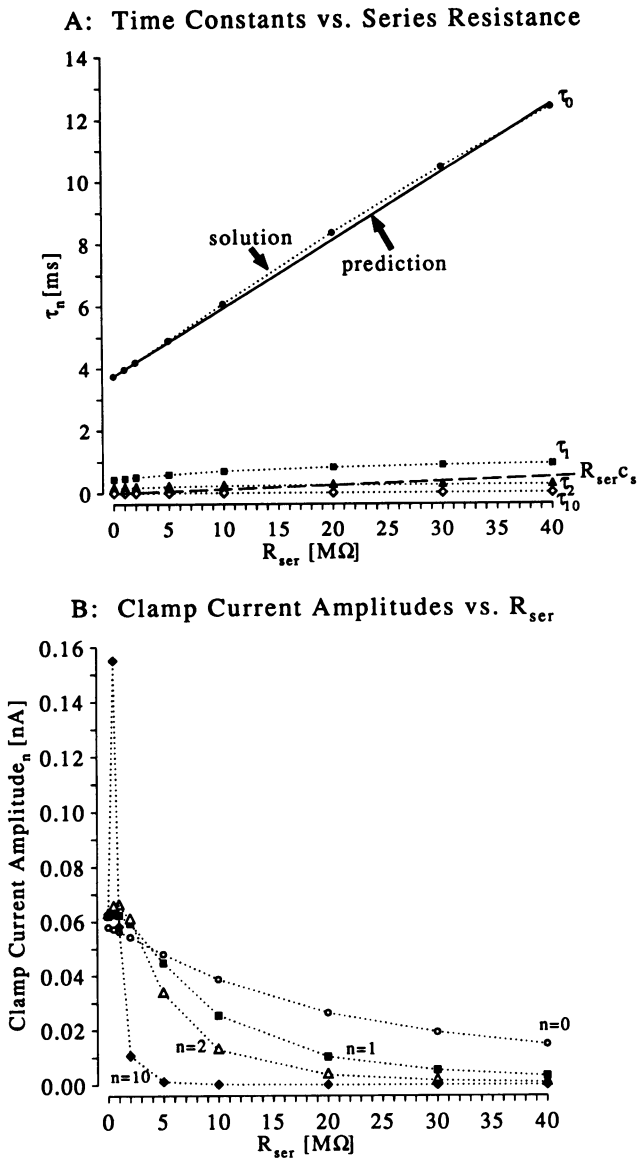


FIGURE 4 Single cylinder + soma model: imperfect voltage clamp. Clamp current for a 1 mV step command to the soma via various series resistances $R_{ser}$. (*A*) changes in the time constants $\tau_0$, $\tau_1$, $\tau_2$, and $\tau_{10}$ with series resistance (*dotted lines*). All the time constants increase with $R_{ser}$, but the faster ones level off more quickly. $\tau_0$ increases linearly with series resistances up to 40 MΩ. The solid line is the increase predicted by Eq. II.58. The "soma alone" charging time constant $R_{ser}C_s$ is also plotted (*long dashed line*), for reference. (*B*) changes in the clamp current amplitude terms with increasing $R_{ser}$. Points joined by dotted lines correspond to amplitudes with the same index (written alongside). All except $n = 0$ show an initial increase, then decrease with $R_{ser}$.

the linear approximation (II.58),[1] the filled circles are the actual values calculated from the analytical solution. A similar linear approximation, with $3\pi$ replacing $\pi$, (except for one of the $\pi$ values in the slope numerator) holds for $\tau_1$ for $R_{ser} < 15$ MΩ (error < 10%). Equivalent approximations for the faster time constants break down at progressively smaller values of $R_{ser}$.

The slower time constants show large fractional changes with $R_{ser}$, although the changes decrease as the time constants become faster. The ratios of the values of the time constants with $R_{ser} = 40$ to their values under perfect clamp are: $\tau_0$: 3.3, $\tau_1$: 2.08, $\tau_2$: 1.62, $\tau_{10}$: 1.16. For $R_{ser} < 40$, $\tau_0$, and $\tau_1$ are never the time constants closest to $R_{ser}C_s$, and yet they show dramatic changes with $R_{ser}$; therefore for this model, Result 2 is clearly incorrect.

In Table 1, the two slowest time constants $\tau_0$ and $\tau_1$ and their ratio $R_\tau$ are listed for models with a number of different $R_{ser}$ values, along with approximate values of $R = R_{sm}/R_{ser}$. It can be seen that two of the models with $R > 100$ result in $\tau_0/\tau_1 > 9$. However, these models do not satisfy the stricter criterion $R > 121/L^2$, so Result 3 appears to hold for this model. (Note the indexing convention: $n$ starts from 0 here, and from 1 in Ref. 3.) The value of $L$ for the model, estimated from Eq. 8 in Ref. 3 is in error by more than 20% for $R_{ser} \geq 10$ MΩ, but by "only" 11% for the $R_{ser} = 5$ MΩ case which satisfies the stricter criterion. The equation gives meaningless answers for $R_{ser}$ above about 20 MΩ, for this model.

The amplitude terms show a complicated dependence on $R_{ser}$, illustrated in Fig. 4 *B*. The 0th amplitude appears to decrease with $R_{ser}$ for all the cases examined. However, all the other amplitudes show an initial increase followed by a decrease as $R_{ser}$ grows. The peak amplitude is both larger and occurs at a smaller value of $R_{ser}$ as $n$, the index of the component, increases.

For each model, the $\tau_n$ closest to $R_{ser}C_s$ is denoted as $\tau_R$. This model time constant $\tau_R$, according to Result 4, should have a much larger associated clamp current amplitude (denoted as $A_R$ here) than both its flanking neighbors $\tau_{R-1}$ and $\tau_{R+1}$. Examination of Table 2 shows that this is clearly not the case. For example, with $R_{ser} = 5$ MΩ (satisfies Jackson's stricter criterion), subscript $_R = 4$, $A_3 = 0.023$ nA, $A_4 = 0.015$ nA, and $A_5 = 0.010$ nA. To reinforce this point, in Fig. 5 each amplitude is plotted against its corresponding time constant using log-log axes, for eight values of $R_{ser}$. The large

**TABLE 1 Single cylinder + soma model: Time constant ratios**

| $R_{ser}$ | $R$* | $\tau_0$ | $\tau_1$ | $\tau_0/\tau_1$ | $L_{est}$‡ |
|---|---|---|---|---|---|
| MΩ | | ms | ms | | |
| 0 | ∞ | 3.749 | 0.446 | 8.41 | 0.447 |
| 0.5 | 8000 | 3.859 | 0.461 | 8.37 | 0.456 |
| 1 | 4000 | 3.970 | 0.475 | 8.36 | 0.464 |
| 2 | 2000 | 4.195 | 0.505 | 8.31 | 0.484 |
| 5 | 800 | 4.891 | 0.591 | 8.28 | 0.496 |
| 10 | 400 | 6.069 | 0.703 | 8.63 | 0.343§ |
| 20 | 200 | 8.349 | 0.825 | 10.12¶ | complex§ |
| 30 | 133 | 10.45 | 0.888 | 11.77¶ | complex§ |
| 40 | 100 | 12.37 | 0.926 | 13.36 | complex§ |

* $R_{sm}/R_{ser}$; should be > 605 by Jackson's strict criterion ($R > 121/L^2$). The lower four models fail this test.

‡ $L$ estimated from $L = (\pi/2)\sqrt{(9 - R_\tau)/(R_\tau - 1)}$, where $R_\tau = \tau_0/\tau_1$.

§ in error by more than 20% from true value of 0.447 space constants.

¶ Ratios exceeding 9 where $R > 100$.

[1] Notation for equations used in this series of three accompanying papers (1, 2). "II.58" refers to Eq. 58 of Paper II.

**TABLE 2 Single cylinder + soma model: Amplitudes of soma charging and adjacent components**

| $R_{ser}$ | $R_{ser}c_s$ | $\overset{*}{R}$ | $\tau_{R-1}$ | $A_{R-1}$ | $\tau_R$ | $A_R^{\ddagger}$ | $\tau_{R+1}$ | $A_{R+1}$ |
|---|---|---|---|---|---|---|---|---|
| MΩ | ms | | ms | nA | ms | nA | ms | nA |
| 1 | 0.013 | 9 | $\tau_8$ 0.016 | $A_8$ 0.086 | $\tau_9$ 0.013 | $A_9$ 0.074 | $\tau_{10}$ 0.010 | $A_{10}$ 0.058 |
| 2 | 0.025 | 6 | $\tau_5$ 0.039 | $A_5$ 0.050 | $\tau_6$ 0.028 | $A_6$ 0.041 | $\tau_7$ 0.021 | $A_8$ 0.031 |
| 5 | 0.063 | 4 | $\tau_3$ 0.106 | $A_3$ 0.023 | $\tau_4$ 0.063 | $A_4$ 0.015 | $\tau_5$ 0.042 | $A_5$ 0.010 |
| 10 | 0.126 | 3 | $\tau_2$ 0.235 | $A_2$ 0.013 | $\tau_3$ 0.113 | $A_3$ 0.007 | $\tau_4$ 0.066 | $A_4$ 0.004 |
| 20 | 0.251 | 2 | $\tau_1$ 0.825 | $A_1$ 0.010 | $\tau_2$ 0.252 | $A_2$ 0.004 | $\tau_3$ 0.117 | $A_3$ 0.002 |
| 30 | 0.377 | 2? | $\tau_1$ 0.888 | $A_1$ 0.005 | $\tau_2$ 0.258 | $A_2$ 0.002 | $\tau_3$ 0.118 | $A_3$ 0.001 |
| 40 | 0.503 | 1? | $\tau_0$ 12.37 | $A_0$ 0.015 | $\tau_1$ 0.926 | $A_1$ 0.003 | $\tau_2$ 0.262 | $A_2$ 0.001 |

* Subscript $R$, index $n$ of time constant $\tau_n$ closest to $R_{ser}c_s$, the "soma-alone" charging time constant. Not to be confused with $R = R_{sm}/R_{ser}$. (? indicates >40% error between $\tau_R$ and $R_{ser}c_s$).

‡ $A_R$ Corresponding clamp current amplitude term (in response to a 1-mV somatic voltage command). First three models satisfy Jackson's "strict" criterion $R > 121/L^2$.

solid triangles are $A_R$ plotted against $R_{ser}c_s$. The $R_{ser}$ value corresponding to each of these is the same as that of the nearest dotted line. It can be seen that in every case shown, rather than standing clearly above its neighbors, as suggested by Jackson's results, $A_R$ actually falls *between* $A_{R-1}$ and $A_{R+1}$. During an experiment it would be hard to distinguish the soma charging component of the response of a cell like the one modelled. Because the soma is much smaller than the dendrites in this case, perhaps this problem is not as serious as it may at first seem. A more thorough assessment should involve fits to noisy waveforms from similar models.

The clamp current waveforms corresponding to the components plotted in Fig. 5 *A* are shown in Fig. 5 *B*. These transients were obtained by summing the first 34 components (down to $\tau_n < 1$ μs) and the steady-state current given in (II.48). The waveforms with $R_{ser} \leq 2$ MΩ superimpose well. However, as $R_{ser}$ increases much above 5 MΩ, the early parts of the transients become visibly reduced. The series resistance at which the current begins to deviate substantially from the perfect clamp case is about the same as the 6.6 MΩ predicted by Jackson's stricter criterion ($R > 121/L^2$) for the break-down in his approximation.

### *Slow capacitance compensation*

It is also suggested (Result 5) that slow capacitance compensation and series resistance compensation can be performed in the "routine" way for amplifiers such as the EPC-7 (List, Darmstadt, Germany). For the purposes of the ensuing discussion, it is assumed that any pipette capacitance is negligible or has been accurately compensated. The slow capacitance compensation circuitry of EPC-7-like amplifiers (e.g., Ref. 25, Fig. 1.14)) is designed to cancel the current charging the lumped membrane capacitance of an *isopotential* cell. For a step voltage command, this is an exponentially decaying current with amplitude $V_{step}/R_{ser}$ and time constant $R_{ser}c_{cell}$, where $c_{cell}$ is the cell capacitance. By adding an amplified, single RC low-pass filtered version of the command voltage, via a capacitor, to the current injected into the pipette, such circuitry effectively subtracts a single exponentially decaying component from the clamp current, when the voltage command is a step. The amplitude of the subtracted current is $V_{step}G_{series}$, where $G_{series}$ is the setting of the G-series dial on the amplifier. The time constant of the subtracted current is $C_{slow}/G_{series}$, where $C_{slow}$ is the setting of the C-slow dial (Ref. 26, pp. 45–46).

According to Ref. 26, the fast transient cancellation procedure is:

(i) Starting with C-slow set at a non-zero value, increase the G-series dial until there is no "jump" between the baseline and the initial current. This ensures that $G_{series} = g_{ser}$.

(ii) Adjust C-slow "to reduce the overall size of the transient" (presumably avoiding "undershoot").

(iii) Turn up the %-COMPensation control, possibly fine tuning the C-slow and G-series settings.

It is also suggested that it is a good idea to observe the transients at "high time resolution," perhaps with 10-kHz filtering.

Simulations of the first two stages of the process are depicted in Fig. 6, for the model with $R_{ser} = 5$ MΩ. Panel *A* shows the responses plotted at a reasonably fast time base, with a sample interval of 0.1 ms (sample rate, 10 kHz). The uncompensated model response is the dotted line labeled "0." The other waveforms are obtained by subtracting from this a single exponential component with amplitude 0.2 nA (correct $G_{series} = 200$ nS) and time constant $R_{ser}C_{slow}$, for a number of values of $C_{slow}$. $C_{slow} = 100$ pF produces obvious undershoot at early times, and is therefore clearly an overcompensation of the soma capacitance.

As C-slow is decreased, the first waveform demonstrating no obvious undershoot is the one with $C_{slow} = 40$ pF. Unfortunately, this is approximately three times the correct soma capacitance of 12.57 pF. Closer examination of the $C_{slow} = 40$ waveform reveals a kink right at the start: perhaps grounds for rejection. If C-slow is decreased still further, the first waveform not showing a kink is the one with $C_{slow} = 30$ pF, still too high.

These overestimates in $c_s$ are potentially serious, not least because they will lead to underestimates of the soma resistance $R_{sm}$ ( $= \tau_m/c_s$) and hence $\rho$, the soma-to-dendritic resistance ratio. This may be one explanation for the surprisingly low $\rho$ of only 1.6 quoted in Fig. 3 of Ref. 3 for a hippocampal CA1 pyramidal cell. The $c_s$ quoted for this cell was 14.9 pF, whereas that of the CA1 pyramidal cell model used below and in the two previous papers was only 6.4 pF.

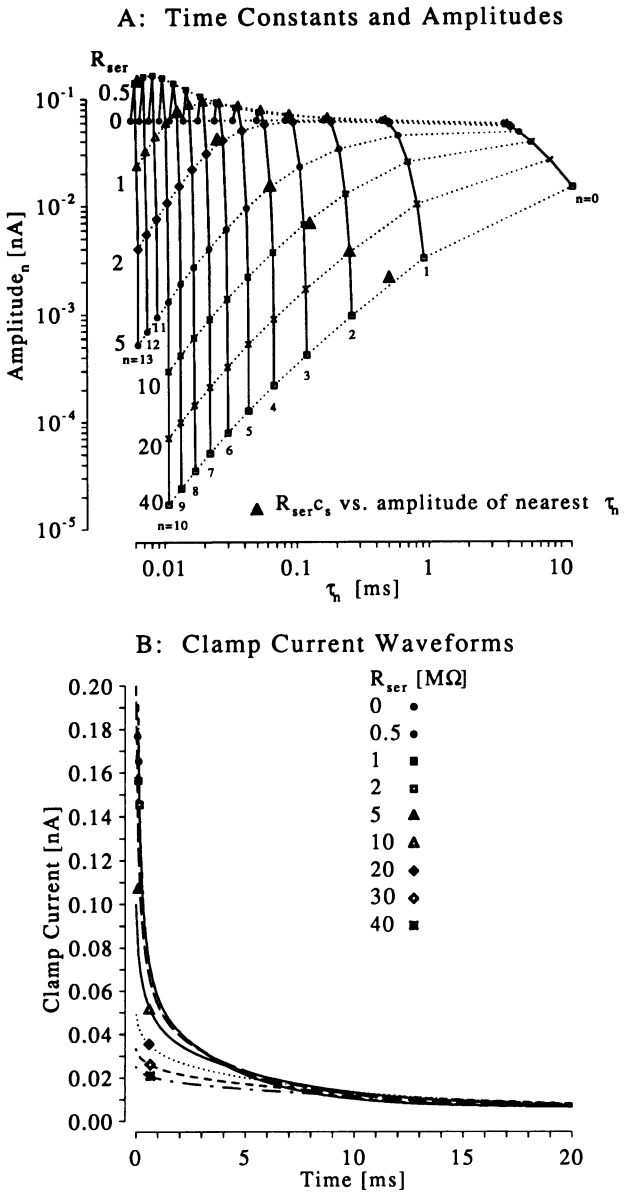


FIGURE 5 Single cylinder + soma model (imperfect clamp), same parameters as before: responses to 1 mV step command. (*A*) clamp current amplitude versus time constant plot (note logarithmic axes). Each clamp current amplitude term is plotted against its time constant, for different values of $R_{ser}$. Points corresponding to the same waveform component using different $R_{ser}$ values are joined with solid lines (the index $n$ of the component appearing below, in *small type*). To guide the reader's eye, components from the same waveform are joined with dotted lines, the series resistance MΩ appearing to the left (in *large type*). For each value of $R_{ser}$, the amplitude of the component with the time constant $\tau_R$ nearest to $R_{ser}c_s$ is plotted against $R_{ser}c_s$ (*large black triangles*), with the exception of the 40 MΩ point, where the amplitude is set to be the average of $A_1$ and $A_2$ (because $R_{ser}c_s$ appears to be mid-way between $\tau_1$ and $\tau_2$). The value of $R_{ser}$ used for each of these is the same as that of the nearest dotted line. Low values of $R_{ser}$ cause the amplitudes of components with intermediate time constants to increase above those of the perfect clamp case. Otherwise, amplitudes decrease with $R_{ser}$ and with $n$. In no case is the amplitude $A_R$ of $\tau_R$ much larger than the amplitudes of the flanking terms (*B*) clamp current waveforms of the same models. The transients from the four models with the lowest $R_{ser}$ values superimpose extremely well. As $R_{ser}$ increases, so the early parts of the waveforms diminish in size, the deviation from perfect clamp becoming obvious for $R_{ser} > 5$ MΩ. Note that initial current = 1 mV/$R_{ser}$.

Other explanations may include dendritic amputations due to slicing, the young age of the rats (1 week), incorrect assumption of cylindrical morphology (see Paper I, Fig. 2), or problems associated with fit nonuniqueness (e.g., Refs. 4 and 5).

Over-estimating $c_s$ could have other unfortunate consequences. In Fig. 6 *A*, the peak current with $C_{slow} = 40$ occurs at 0.6 ms, whereas the peak for $C_{slow} = 12.57$ is earlier, at 0.2 ms. Whether or not additional series resistance compensation is carried out, the $C_{slow} = 40$ peak will always be after the $C_{slow} = 12.57$ peak. When attempts are made to fit model responses or multiple exponentials to experimental data, a decision has to be reached about when to start the fit interval.

If *direct fitting* of model responses to the data is being attempted, it is necessary to start at the peak, or just after (e.g., when the waveforms have positive early components as judged from semi-log plots), because in response to positive step commands, all the amplitude terms in the clamp current analytical solution are positive (see Paper II, comments below Eq. II.47). Failure to do this may result in serious errors in the estimated model parameters as the fit program attempts to "drag down" the early parts of the model response.

At first sight it should be possible to circumvent this problem by fitting exponentials to some or all of the time course of the transient, allowing negative amplitudes. If, however, as with the $R_{ser} = 2$ model considered above (see Table 2), $R_{ser}c_s$ is roughly midway between two $\tau_n$ values, the slow capacitance compensation procedure will have contributed another distinct (negative) exponential component to the waveform. At best, all a good exponential fitter can do is to "uncompensate" such target waveforms: if it correctly extracts one time constant of $C_{slow}R'_{ser}$ (where $R'_{ser}$ is the remaining, uncompensated series resistance) and a corresponding amplitude of $-V_{step}/R'_{ser}$, then little will have been accomplished by the slow capacitance compensation. At worst, the fitter might misleadingly combine a number of components which should really be distinct.

For the above reasons, it seems prudent to use intervals *after* the peak with both direct and multiexponential fits. It follows that accidentally setting C-slow too high will lead to later intervals than with the correct setting, and hence less waveform information to constrain the fit.

It is possible that the overestimation of $c_s$ in Fig. 6 *A* was a result of not using a fast enough time base. The bandwidth of the EPC-7 is 100 kHz (see Ref. 26, preliminary specification at end). The simulations were repeated, sampling at 200 kHz and slow capacitance compensation was carried out as before. The first 0.2 ms of selected waveforms are plotted in Fig. 6 *B*. At this extremely fast time base, it can be seen that the $C_{slow} = 30$ waveform actually does demonstrate undershoot after all, but the current is already positive by $t = 0.04$ ms. The first nonundershooting waveform now is with $C_{slow} = 15$ pF, only a 20% overestimate of the correct value.

Providing the fastest possible time base is used, overestimation of $c_s$ may largely be avoidable. However, given the

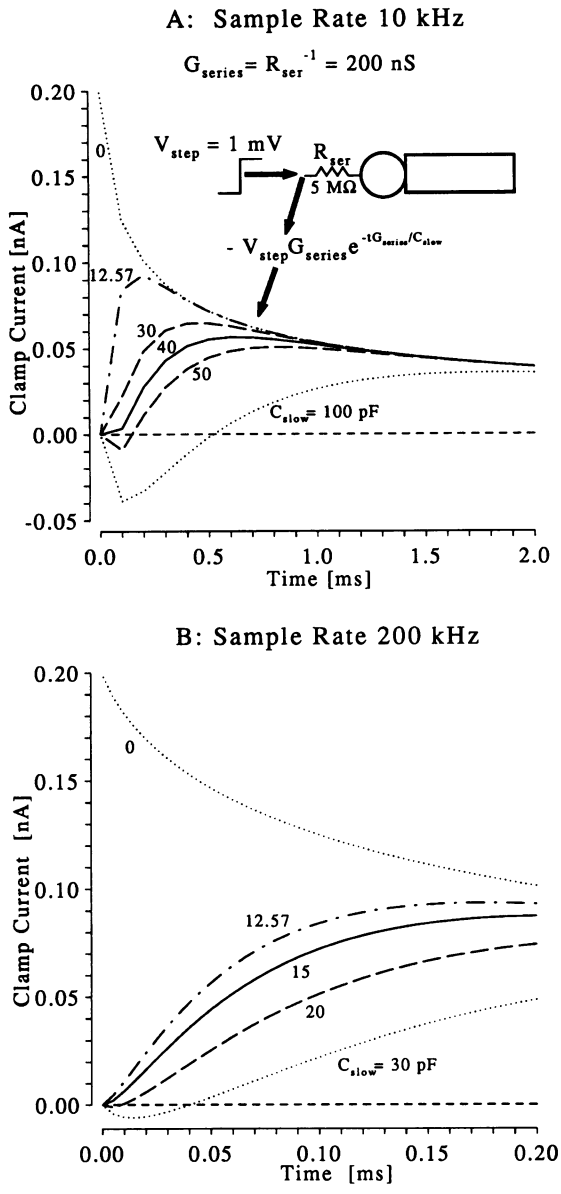


FIGURE 6 Subtractive capacitance compensation illustrated for the single cylinder + soma model with a series resistance of 5 MΩ. The effects of adjusting the G-series and C-slow dials on an amplifier such as the EPC-7 are simulated, for a step command, by subtracting from the clamp current response a single exponential, with amplitude $V_{step}G_{series}$ and time constant $C_{slow}/G_{series}$. Each trace is marked with the $C_{slow}$ used. The uncompensated response is the dotted line marked "0": its initial current is $V_{step}/R_{ser}$ = 0.2 nA. (*A*) sample rate of 10 kHz. The correct setting, with $C_{slow} = c_s$ = 12.57 pF, is the dot-dashed line. Turning C-slow up to 100 pF (*lower dotted line*) causes an obvious undershoot in the response, suggesting overcompensation. Without prior knowledge of $c_s$ it is hard to say what the correct adjustment is: the setting which just avoids undershoot at this sample rate (10 kHz) is 40 pF (*solid line*), although there is a slight kink in the rising phase. The slight undershoot with 50 pF might be missed with a slower sample rate. (*B*) Sample rate of 200 kHz. Note expanded time axis. The C-slow setting just avoiding undershoot is now $C_{slow}$ = 15 pF (*solid line*). $C_{slow}$ = 20 pF shows slight undershoot (*long dashed line*: first sample point only) and undershoot can now be seen clearly with $C_{slow}$ = 30 pF (*lower dotted line*).

existence of an exact analytical solution for this situation, incorporating both soma capacitance and series resistance, perhaps it would be better to adopt a different approach: that of direct fitting *without* slow capacitance compensation. It may still be advantageous, however, to perform series resistance compensation. In order to do this without C-slow compensation on an EPC-7, the G-series dial must be set correctly, and then C-slow must be turned down as low as possible before turning up the %COMPensation dial.

It is not surprising, on purely theoretical grounds, that the approach advocated by Jackson should run into trouble in some cases. As discussed in Paper II, the components of the cell linked in parallel at the end of the series resistance can be separated. Each component can be individually subjected to the voltage command step. When $R_{ser} > 0$, the sum of their clamp currents is *not* equal to the clamp current into the intact cell. Because of this *nonsumming interaction*, it is not possible to compensate for one cell component (e.g., the soma capacitance) by a purely *subtractive* procedure like that considered above.

Attempts to separate the soma capacitance from the proximal dendritic capacitance may be inappropriate for another reason: it is quite often difficult to define precisely where the "soma" ends in many classes of neurone, for example, "thick" layer V visual cortical pyramidal cells (23) and CA3 pyramidal cells in rats (Refs. 5 (Chapter 6) and 15). Moreover, as discussed in Paper II (Parameter Dependence of Imperfect Clamp Impulse Response section), the distorting effect of $R_{ser}$ depends on the electrical and morphological parameters of the model, being worse when more dendritic capacitance is electrically "close" to the soma, e.g., when $R_i$ is relatively low. "Effective" (soma + proximal dendritic) capacitance blends imperceptibly into "shielded" (distal dendritic) capacitance in a way that depends on the model parameters, and the time course and location of the input (Ref. 5, Chapter 6).

### *Other problems*

The methods in Ref. 3 suffer from serious additional problems of *fit nonuniqueness*, common to all techniques involving the matching of noisy experimental transients to a model waveform (e.g., Ref. 5, Paper I). This fit nonuniqueness is particularly bad with unconstrained exponential fitting, a technique in common use in the field of passive neurone modelling. When no additional constraints are imposed on the values that the amplitudes and time constants can take, a range of "acceptable" fits can be obtained with $L$ taking values anywhere between 0 and ∞ (G. Major, unpublished observations). To some extent this problem is overcome by imposing other constraints such as plausible limits on the parameters (e.g., Ref. 5) or amplitude and time constant ratios (see Paper II). In addition, recourse to *direct* fitting can build in all the constraints inherent in a particular model, and hence can restrict the range of acceptable parameters considerably.

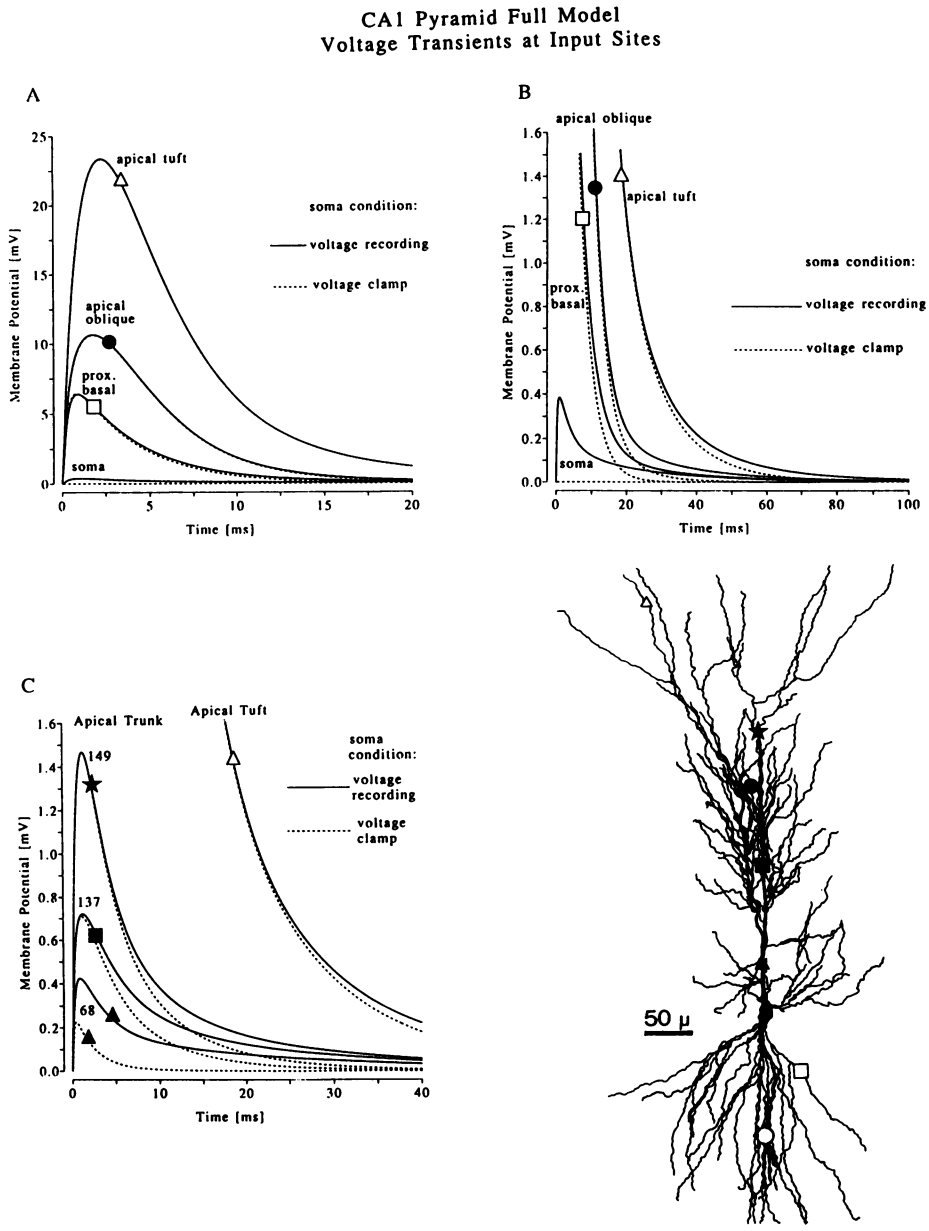


FIGURE 7 CA1 Pyramidal cell. The *camera lucida* drawing from Paper I, Fig. 2, is reproduced here, with the seven input sites in Table 3 marked approximately (segment numbers in parentheses as follows). △, apical tuft (110); ★, apical trunk (149); ●, apical oblique (146); ■, apical trunk (137); ▲, apical trunk (68); □ proximal basal (16); ○ mid basal (44). Only the full geometry was considered (with all spines collapsed). The electrical parameters were as in Paper I: $C_m = 0.7$ $\mu Fcm^{-2}$, $R_m = 100,000$ $\Omega cm^2$, $R_i = 200$ $\Omega cm$ and $g_{shunt} = 15$ nS. The input current was the same as in Paper I, Fig. 6: total charge 0.1 pC, double exponential function, $\tau_{sy_1} = 0.1$ ms, $\tau_{sy_2} = 2$ ms. To obtain each waveform, this current was injected into the indicated site, and the voltage at the same point was recorded, either with somatic voltage recording or with the soma perfectly voltage clamped to zero. (*A*) input site voltage transients at the soma and at three positions on thin dendrites. The early parts of the dendritic transients are virtually unaffected by clamping. (*B*) the same waveforms out to later times, with the voltage axis expanded. At late times, return to baseline is more rapid with voltage clamp. (*C*) input site voltage transients at three positions along the apical trunk (a relatively thick structure) compared with that from the apical tuft. Again, clamping hardly affects the peaks, but does speed the return to baseline. An exception is the response in segment 68 which is only 0.019 λ from the soma: it is so close electrically that under voltage *recording*, the response is virtually the same as the somatic response to a somatic input (shown in *A* and *B*).

In summary, the procedure outlined by Jackson (3) should be adopted with some caution, as stated by that author, when it is suspected that $\rho_\infty$ is high. Values of the order of 50 or more are likely to cause problems with most pyramidal cells, although a more systematic assessment needs to be performed.

## EXAMPLE 2: HIPPOCAMPAL CA1 PYRAMIDAL CELL

In this section, the hippocampal CA1 pyramidal cell introduced in Paper I is modelled using the voltage clamp and voltage recording waveform generator programs, to explore further the following issues: (*a*) voltage clamp control of subsynaptic voltage swings, (*b*) cable and series resistance effects on synaptic clamp currents, (*c*) parameter dependence, and (*d*) propagation of voltage commands.

The morphology of the cell is shown in Paper I, Figs. 2 (full model) and 4 (cartoon representation). The default electrical parameters are (as before): $C_m = 0.7$ $\mu Fcm^{-2}$, $R_m = 100,000$ $\Omega cm^2$, $R_i = 200$ $\Omega cm$, $g_{shunt} = 15$ nS (loosely based on fitting the model to the real cell's short pulse response: see Paper I).

### Case I: Clamping synaptic inputs

#### *Causes for concern*

Because of the interest in long-term potentiation, a large number of voltage "clamp" studies have been undertaken on the Schaeffer collateral inputs onto hippocampal CA1 pyramidal cells (for example, see Refs. 17, 27–32). Preliminary simulations of mossy fiber synaptic conductances onto a CA3 pyramidal cell from a 19-day-old rat (Refs. 5 (Chapter 6) and 15) have shown that even these relatively proximal

**TABLE 3 CA1 pyramid input sites**

| Location | Full model | | | | Cartoon | | |
|---|---|---|---|---|---|---|---|
| | Segment | $x$ ($\mu$m) (no spines*) | $x$ ($\mu$m) (spines‡) | $X$¶ ($\lambda$) | Segment | | $x$ ($\mu$m) |
| Proximal basal (□) | 16 | 14.9 | 30 | 0.092 | 2 | | 65 |
| Mid-basal (○) | 44 | 109.5 | 200 | 0.247 | 3 | | 214 |
| Apical trunk (▲) | 68 | 16.6 | 20 | 0.019 | | ND§ | |
| Apical trunk (■) | 137 | 5.9 | 10 | 0.113 | | ND§ | |
| Apical trunk (★) | 149 | 80.3 | 127 | 0.230 | | ND§ | |
| Apical oblique (●) | 146 | 78.5 | 158 | 0.300 \|\| | 26 | | 0 |
| Apical tuft (△) | 110 | 116.9 | 200 | 0.648 | 19 | | 81 |

* Actual measured physical distance from proximal end of segment in real neurone.

‡ Distance along segment in model after spine collapse procedure, i.e., measured distance $\times F^{2/3}$, where for a given segment, $F$ is the area with spines divided by area without spines.

¶ Total electrotonic distance from soma.

§ ND, not done.

|| 0.285 in cartoon.

inputs may suffer considerable attenuation and smoothing due to dendritic cables. Moreover, because of the large size of these cells, even quite low series resistances can produce serious additional distortions. CA1 pyramids and CA3 pyramids are similar in many respects, both in their morphology and their electrophysiology. The majority of Schaeffer collateral synapses onto CA1 cells occur at locations more distal than the mossy fiber zone in CA3. One would therefore expect voltage clamp to be even worse for Schaeffer collateral inputs than for mossy fiber inputs.

### *Subsynaptic voltage transients*

Seven dendritic input sites, marked on the *camera lucida* drawing in Fig. 7, were selected (see legend and Table 3 for details). The same double exponential current as used in Paper I was injected into each site in turn, directly into the dendritic shaft (not into a spine). The current parameters were: total charge 0.1 pC, $\tau_{sy_1}$ 0.1 ms, $\tau_{sy_2}$ 2 ms. In Paper I, Fig. 6, it was shown that this input, when injected into the apical oblique site (●), gave rise to an 120 $\mu$V peak synaptic potential at the soma. This is comparable to the typical quantal amplitude of Schaeffer collateral excitatory post synaptic potentials (EPSPs) recorded with sharp electrodes (33).

Local voltage transients were recorded at the injection ("subsynaptic") sites, under two conditions: (i) *voltage recording* at the soma, with a shunt (as in Paper I), and (ii) *perfect voltage clamp* to zero at the soma.

In this model, (i) is also equivalent to imperfect voltage clamp to zero via an $R_{ser}$ of 66.6̇ MΩ, since $g_{shunt}=15$ nS. See Paper II (Comparison to Voltage Recording with a Shunt section) for an explanation.

It is interesting to compare the waveforms: at early times, except in the case of very proximal inputs (into the soma and into segment 68 on the apical trunk), there is virtually no difference between the transients produced under the two conditions. Removing the shunt also has virtually no effect on the peaks (not shown). Considering the imperfect clamp interpretation of (i), it can also be seen that series resistance compensation (i.e., reducing $R_{ser}$ from 66.6̇ MΩ to zero) will have a negligible effect on peak subsynaptic voltages.

Inputs of 0.1 pC into thin segments (Fig. 7 *A*) produce large transients of between 5 and 25 mV at the input site. (The diameters, with spines collapsed, were: proximal basal (segment 16) and apical oblique (segment 146) = 0.78 $\mu$m, apical tuft (segment 110) = 0.60 $\mu$m). (If input spines had been included explicitly in the model, the spine head transients would have been even larger than these shaft voltage swings.) Compared with proximal inputs, distal inputs produce transients that are both bigger and peak later: the "escape route" for charge redistribution is both longer and narrower; more charge is bottled up for more time. At late times ( $>$ 20 ms), voltage clamp does cause a more rapid decay to baseline (Fig. 7 *B*) than that experienced under voltage recording. If the shunt is removed, the final decay is even slower (not shown).

If the cartoon or any other simplified representation is used to model subsynaptic voltage transients, the input segment must not be collapsed together with any others. If it is, the local voltage swing will be too small, because of the reduced local input resistance. Moreover, the clamp will appear to be more effective, because the attenuation of the voltage *en route* to the soma is less than in the full model, resulting in more effective voltage feedback between the clamp amplifier and the input site. Fortunately, however, the clamp *current* from the cartoon representation provides a good approximation to that from the full model (see below). In fact, if Rall's 3/2 rule applies, the clamp current from the branched model is identical to that from the equivalent cylinder representation.

Fig. 7 *C* shows the responses at three stimulation sites along the apical trunk, a wide structure (diameters with spines collapsed: segment 68 = 3.8 $\mu$m, segments 137 and 149 = 3.2 $\mu$m). Under voltage recording, the soma response to a somatic input in Fig. 7 *B* is almost indistinguishable from the transient recorded from segment 68 in response to an input at the same point in segment 68 (Fig. 7 *C*), only 0.019 space constants away from the soma. The apical tuft response

**TABLE 4 CA1 pyramid waveform measures (full model only)**

| Input site | $V_{peak}$* | Efficacy | $t_{peak}$ | $\int_0^\infty V dt$ | Efficacy | $t_{1090}$ | Half-width |
|---|---|---|---|---|---|---|---|
| | μV | % | ms | mVms | % | ms | ms |
| A. Postsynaptic potentials (somatic voltage recording with shunt) | | | | | | | |
| Soma | 385 | 100 | 1.0 | 4.80 | 100 | 0.5 | 5.4 |
| Proximal basal (□) | 220 | 96 | 2.9 | 4.62 | 96 | 1.3 | 13.5 |
| Mid-basal (○) | 191 | 50 | 5.6 | 4.50 | 94 | 2.9 | 16.0 |
| Apical oblique (●) | 123 | 32 | 9.6 | 4.15 | 86 | 4.9 | 26.5 |
| Apical tuft (△) | 75 | 19 | 20.4 | 3.55 | 74 | 10.1 | 40.9 |
| Input site | $i_{peak}$ | Efficacy | $t_{peak}$ | Charge‡ | Efficacy | $t_{1090}$ | Half-width |
| | pA | % | ms | pC | % | ms | ms |
| B. Voltage clamp currents | | | | | | | |
| Soma | 42.7 | 100 | 0.3 | 0.100 | 100 | 0.2 | 1.8 |
| Proximal basal (□) | 17.2 | 40 | 1.2 | 0.096 | 96 | 0.6 | 4.4 |
| Mid-basal (○) | 11.9 | 28 | 3.4 | 0.094 | 94 | 1.8 | 6.7 |
| Apical oblique (●) | 6.3 | 15 | 5.5 | 0.086 | 86 | 2.8 | 11.4 |
| Apical tuft (△) | 2.9 | 7 | 12.1 | 0.074 | 74 | 6.0 | 22.1 |

* Glossary: $V_{peak}$, peak soma voltage; $i_{peak}$, peak clamp current; $t_{peak}$, time to peak; $t_{1090}$, 10 to 90% rise time; half-width, width at half maximum amplitude.
‡ Charge transferred to soma = time integral of current waveform.

from Fig. 7 *B* is also included for comparison. Only segment 68 shows a marked difference in its peak response between voltage recording and voltage clamp. The other trunk segments, although producing smaller transients than the thinner segments in Fig. 7 *A*, show the same pattern: again the peak voltage swing is virtually unaltered by the clamp, but at late times decay to baseline is more rapid.

In order to achieve good agreement between analytical solution and compartmental model waveforms, extremely fine compartmentalization was required in the latter. This is because voltage transients travelling along a cable attenuate very steeply when one end is clamped. An intuitive explanation is that the clamp condition maximizes the degree of charge redistribution, and hence the extent to which the cable is "experienced" by the transient.

The important conclusion to be drawn from these simulations is that *with fast synaptic currents, voltage clamp is surprisingly ineffective at controlling the local membrane potential at most input sites*, except those extremely close to the clamp point. This conclusion is robust with respect to the electrical parameters (see below).

### *Synaptic potentials and "synaptic" clamp currents*

In Fig. 8, the waveforms at the soma resulting from the somatic and non-trunk inputs are compared for voltage recording (with a shunt, see above) and perfect somatic voltage clamp. Along with the waveforms from the full model are those from the cartoon, with injection sites as in Paper I, Fig. 4, at points electrically equivalent to those in the full model (i.e., at the same electrotonic distance from the soma, except for the input into the uncollapsed apical oblique, whose origin has been shifted slightly toward the soma in the cartoon). In Fig. 8 *A* are shown synaptic potentials obtained from the models under voltage recording. The corresponding clamp currents, with the soma voltage perfectly clamped to zero, are shown in Fig. 8 *B*. Notice the expanded time scale in *B*: the clamp currents are appreciably faster than the synaptic potentials.

It can be seen that there is close agreement between the waveforms generated by the two models, although the cartoon output (except the somatic EPSP) is slightly larger and peakier, as if the inputs were a little closer in electrical terms to the soma. The transients are virtually identical to equivalent compartmental model output (with 99 compartments/space constant). As in Paper I, the cartoon ran faster than the full model, by a factor of over 200.

With these electrical and morphological parameters, the dendritic trees are capable of substantial smoothing and attenuation of the synaptic inputs. Table 4 lists the following waveform measures for the different full model transients: peak voltages and currents, time integrals (i.e., charge transfer in the case of the currents), relative efficacies (these values, divided by the corresponding measure for a somatic input), 10–90% rise times and half-widths. In the most extreme case, the apical tuft input, the 10–90% rise time of the current has been slowed from 0.2 to 6.0 ms, the peak current is reduced to 7% of its original value at the synapse, and the charge transferred to 74% of that of a somatic input. For the corresponding synaptic potential in the voltage recording case, the 10–90% rise time is slowed from 0.5 ms (somatic input) to 10.1 ms, and the peak voltage efficacy is 19%. The time integral relative efficacies are the same under voltage clamp and simple voltage recording, and are identical to the steady-state relative efficacy (e.g., see Ref. 34, pp. 779–780, and Paper I, Appendix 3, Eq. I.111). However, the peak voltage efficacies with voltage recording are always greater than the peak current efficacies under voltage clamp: as explained above, the filtering effects of the cable are experienced more strongly with voltage clamp than with voltage recording.

### *Parameter dependencies of subsynaptic voltage and clamp currents*

The results in Paper II, (Parameter Dependence (Perfect Clamp) section) suggest that the conclusions in the previous two sections will depend only weakly upon the parameter

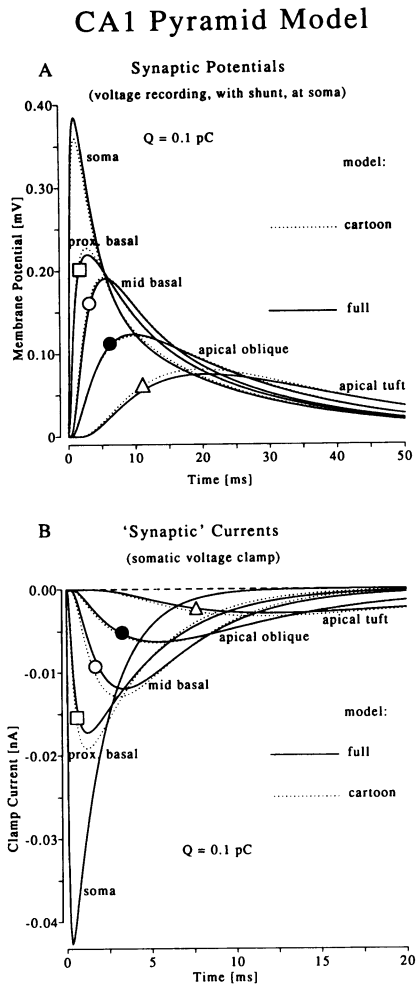


FIGURE 8 CA1 pyramidal cell, full model and cartoon compared: responses at the soma to currents injected at the soma or at the non-trunk locations in Table 3, under voltage recording with a 15-nS shunt (*A*), and perfect voltage clamp to zero (*B*). For the cartoon representation, the sites of the non-trunk inputs are marked with the same symbols as in Table 3 and Paper I, Fig. 4. Note faster time scale in *B*. As before, total charge = 0.1 pC, double exponential function, $\tau_{sy_1}$ = 0.1 ms, $\tau_{sy_2}$ = 2 ms. Waveform parameters are listed in Table 4. With the electrical parameters used (see previous figure legend), the dendritic cables have a marked attenuating and smoothing effect on the inputs. The clamp current transients are both briefer than the corresponding synaptic potentials under voltage recording, and have lower peak efficacy. Note that the clamp current transients under imperfect clamp with $g_{ser}$ = 15 nS ($R_{ser}$ = 66.6 MΩ) would be the same as the waveforms in *A* multiplied by −15 nS.

$R_m$: all of the time constants and amplitudes of the fast exponential components in the synaptic voltage swing are relatively insensitive to $R_m$, even after inclusion of the extra factors resulting from convolution with the input function. The faster time constants are roughly proportional to $R_i$, so although the impulse response amplitudes are independent of $R_i$, the double exponential response amplitudes are not: this is clear from inspection of Eq. I.52.

The results of making 2-fold changes to each of the electrical parameters in turn are illustrated in Fig. 9 for the apical oblique input under perfect somatic voltage clamp. The plots confirm that the early parts of the responses are insensitive to changes in $R_m$ (see also Refs. 35 and 36 (pp. 41–42)): both the peak subsynaptic voltage swing and the peak clamp current are virtually unchanged. This suggests that maneuvers intended to increase $R_m$ to improve the efficacy of voltage clamp are likely to be of limited success (as pointed out in Ref. 8).

Halving $R_i$ to a more "traditional" value of 100 Ωcm reduces the peak voltage swing and increases the peak clamp current. Both waveforms are also appreciably faster (as expected). However, the cable still has an appreciable filtering effect (compare the clamp current with the actual synaptic current in Fig. 8 *B*, marked "soma"). Again, voltage clamp hardly reduces the peak subsynaptic voltage swing when compared with voltage recording (not shown). A doubling of $C_m$ also produces qualitatively the effects predicted from the impulse response dependencies: reduced amplitudes and slower waveforms.[2] Changes in $g_{shunt}$ of course have no effect, because the soma is perfectly clamped to zero. With voltage recording at the soma, however, changes in $g_{shunt}$ alter the final decay (but not the early parts) of the subsynaptic waveforms: for example, see Fig. 7, where in effect the shunt is varied between 15 nS and infinity (perfect voltage clamp).

The parameters selected span much of the biological range of interest (e.g., Refs. 4, 5, and 15), and the conclusions about the inadequacy of voltage clamp apply in every case. It is quite possible that $R_i$ is even higher than the 200 Ωcm used as a default here (e.g., Refs. 4, 5, 24, and 37). A higher $R_i$ would lead to more cable smoothing of the clamp current and to less effective clamping of dendritic input sites.

### *Effects of series resistance on measured clamp currents*

As discussed in Paper II, and in Example 1 above, cable effects and series resistance effects compound one another, and are dependent on: (i) the detailed morphology, (ii) the electrical parameters, (iii) the input kinetics, and (iv) the input location (see also Ref. 5 (Chapter 6)). Because of this, *detailed models of each particular experimental system* need to be made in order to assess the likely errors introduced by the combination of poor space clamp and imperfect voltage clamp.

[2] Interestingly, the first millisecond or so of the subsynaptic voltage waveforms from two of the models, that with $C_m$ = 1.4 and that with $R_i$ = 100, superimpose exactly. Both models have the same $R_i/C_m$ ratio. At very early times, virtually no charge has reached either end of the input segment, so it can be approximated by an infinite cable. Rearranging Eq. 3.48 of Ref. 36, which gives the charge impulse response of an infinite cable, setting $X = 0$ (stimulating site = recording site) and $Q = 1$ (unit charge), we obtain

$$V = \frac{R_i^{1/2}}{C_m^{1/2} d^{3/2} \pi^{3/2} t^{1/2}} e^{-t/\tau_m}. \quad (4)$$

When $t \ll \tau_m$, the exponential term simplifies to 1. It can be seen that models with the same $R_i/C_m$ ratio will give the same sub-synaptic voltage response over these times, and this will also be true after convolution with the input function used here.

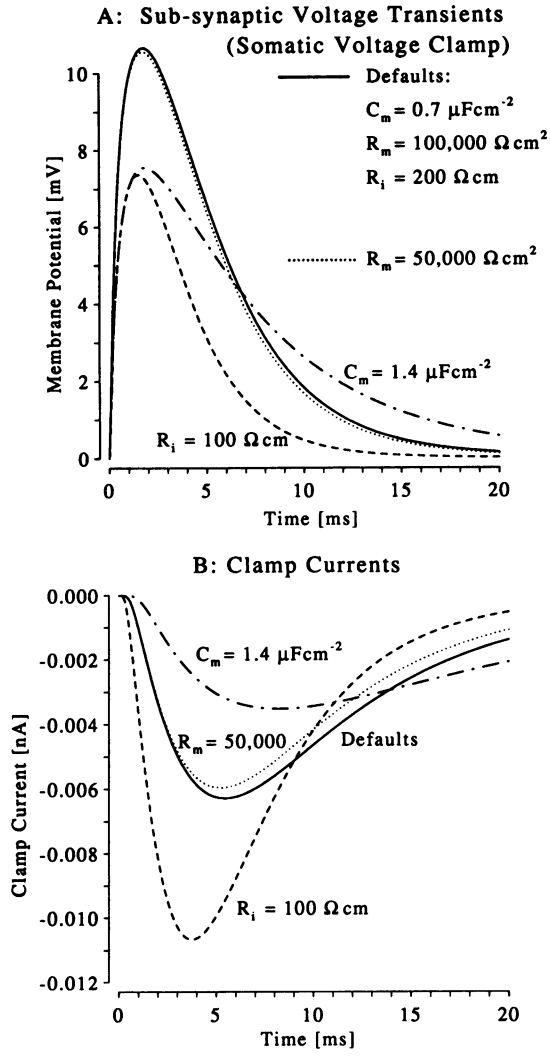


FIGURE 9 CA1 pyramidal cell full model: illustration of the parameter dependence of the apical oblique responses from the previous figures, under *perfect somatic voltage clamp*. Four models are compared: the "default" model (*solid line*) with the electrical parameters shown in *A*, and three other models, each with one parameter altered by a factor of 2 from the default: $R_m$ halved (*dotted line*), $R_i$ halved (*dashed line*), $C_m$ doubled (*dot-dash line*). (*A*) voltage transients at input site (segment 146: 158 μm). (*B*) clamp currents recorded at the soma. Changing $R_m$ has virtually no effect on the waveforms. Halving $R_i$ speeds both responses, reducing the peak voltage swing and increasing the peak clamp current. Doubling $C_m$ slows and attenuates both responses. Interestingly, the very early parts of the $C_m$ = 1.4 and the $R_i$ = 100 voltage responses in *A* are nearly identical (see Footnote 2 for explanation).

A preliminary attempt at this has been carried out for simulated Schaeffer collateral inputs into the CA1 cell model. Two input sites were selected: a very proximal location on the apical trunk (segment 68: Fig. 7, ▲), and the apical oblique site in previous figures (half way along segment 146: ●). The first is closer to the soma than the vast majority of probable Schaeffer synapses, and is intended to represent the *best plausible case* for space clamping. The second is intended to represent a *typical* Schaeffer collateral input. Many other Schaeffer inputs arrive even further (electrically) from the soma, and will consequently suffer even more cable distortion.

The input current parameters were as above: slower currents would lead to less severe and faster currents to more severe distortions (see Example 1). The default electrical parameters were those used above, except that $g_{shunt}$ was set to zero, instead of 15 nS, to mimic more closely the probable situation with whole-cell recording (e.g., Refs. 5 (Chapter 6), 38–40). A range of values of series resistance between 0 and 100 MΩ were explored. In addition, a model with a more "traditional" value of $R_i$ of 70 Ωcm was tested, as well as one with a lower $R_m$ of 40,000 Ωcm$^2$. The latter model had a $\tau_m$ of 28 ms which is consistent with those recorded from adult guinea pig CA1 neurones at rest using the nystatin patch method (40). It can be seen from Fig. 9 *B* that raising $C_m$ from 0.7 μFcm$^{-2}$ would lead to increased distortion of the clamp currents with perfect clamp. In addition, the series resistance effects would become worse (see Paper II, Parameter Dependence of Imperfect Clamp Impulse Response section).

The results of the simulations are summarized in Fig. 10. In Fig. 10 *A* the clamp current waveforms for the two input locations with the default electrical parameters are compared to the actual input current ("Soma" measurement) for three sample values of series resistance: 0 (perfect clamp), 2 MΩ, achievable with whole cell recording using the cleaning method (e.g., Refs. 15 and 38), and 20 MΩ, which can be achieved routinely with the "blind" method (e.g., Refs. 18 and 41) or the perforated patch method with partial series resistance compensation (based on series resistances in Refs. 32 and 40). The clamp current waveforms from both dendritic inputs are seriously smoothed and attenuated by the cable alone (in agreement with the previous simulations). Any series resistance worsens the distortions, particularly for the less smoothed proximal input.

The other three panels of Fig. 10 summarize waveform measures for all three models over the full range of series resistances investigated. The relative peak current "efficacy" (measured ÷ actual) is shown in Fig. 10 *B*. The efficacy is worse for the midoblique input than for the trunk input (14.7 vs. 72%, default model with $R_{ser}$ = 0, falling to 8.5 and 26.1%, respectively, with $R_{ser}$ = 20 MΩ). The proximal to midoblique difference is smaller for the low $R_i$ model. Changing $R_m$ has virtually no effect (consistent with results above). The fall-off with increasing series resistance is worse for the trunk input than the oblique input. The fall-off is also worst for the low $R_i$ model, because more of the dendritic capacitance is "exposed to" the clamp amplifier. These simulations suggest that the Schaeffer collateral quantal conductances measured experimentally (e.g., Refs. 27–32, 42), which typically are in the range 30–70 pS, may be serious underestimates of the true conductances, perhaps by as much as an order of magnitude.

Fig. 10 *C* shows the 20–80% rise times of the clamp currents, compared with the 0.11-ms rise time of the input cur-

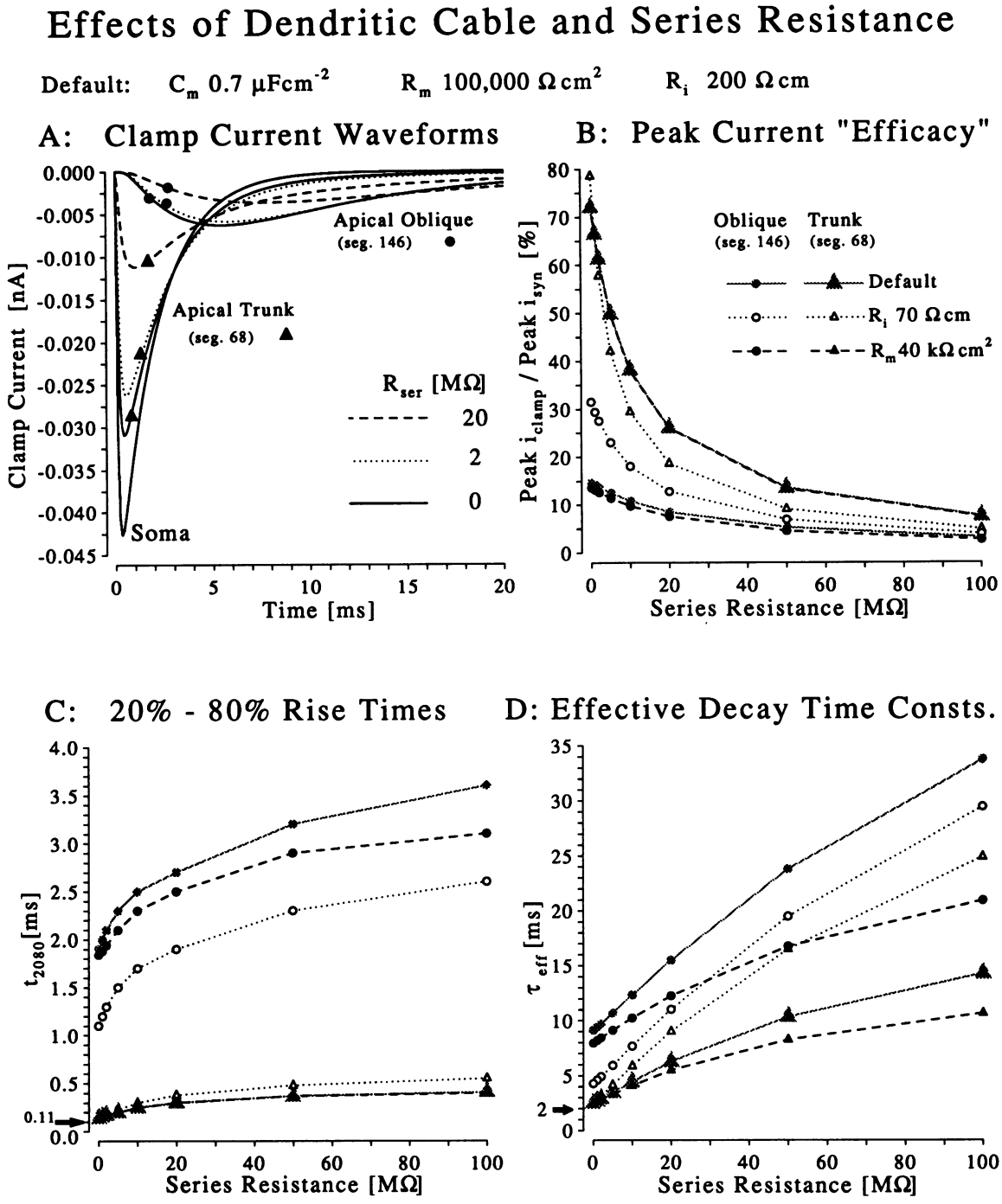


FIGURE 10 CA1 pyramidal cell, full model: the combined filtering effects of the dendritic cable and the series resistance on the clamp currents recorded in response to simulated Schaeffer collateral inputs. The current parameters and model morphology were as specified in the legend of Fig. 7. Two of the input locations shown in Fig. 7 were selected, the proximal apical trunk site (*filled triangles*, segment 68, an "optimistic" position for a Schaeffer collateral input) and the slightly distal-of-mid apical oblique site (*filled circles*, segment 146, half way along, a typical likely position). Three models were tested, all with $C_m = 0.7\ \mu Fcm^{-2}$ and $g_{shunt} = 0$ nS. The default $R_m$ and $R_i$ were 100,000 Ωcm$^2$ and 200 Ωcm, respectively. (*A*) clamp current waveforms $i_{clamp}$ from the default model, compared to the actual input current $i_{syn}$ (marked "Soma"), for three values of series resistance 0 (*solid line*), 2 MΩ (*dotted line*), and 20 MΩ (*dashed line*). (*B–D*) clamp current waveform measures versus series resistance, for all three models. Default, grey symbols; $R_i$ = 70 Ωcm, open symbols; $R_m$ = 40, 000 Ωcm$^2$, black filled symbols. Circles correspond to the the oblique input, and triangles to the trunk input. (*B*) peak current efficacy (i.e., measured clamp current/actual synaptic current): notice that the efficacies of the trunk input superimpose almost exactly for the default and $R_m$ = 40, 000 models. (*C*) 20–80% rise times. Again the default and $R_m$ = 40, 000 models' trunk inputs superimpose. The actual $t_{2080}$ of the synaptic current is arrowed. (*D*) effective decay time constants, fitted between peak + 0.7 ms and peak + 20 ms. The actual decay time constant $\tau_{sy_2}$ = 2 ms of the synaptic current is indicated by the arrow.

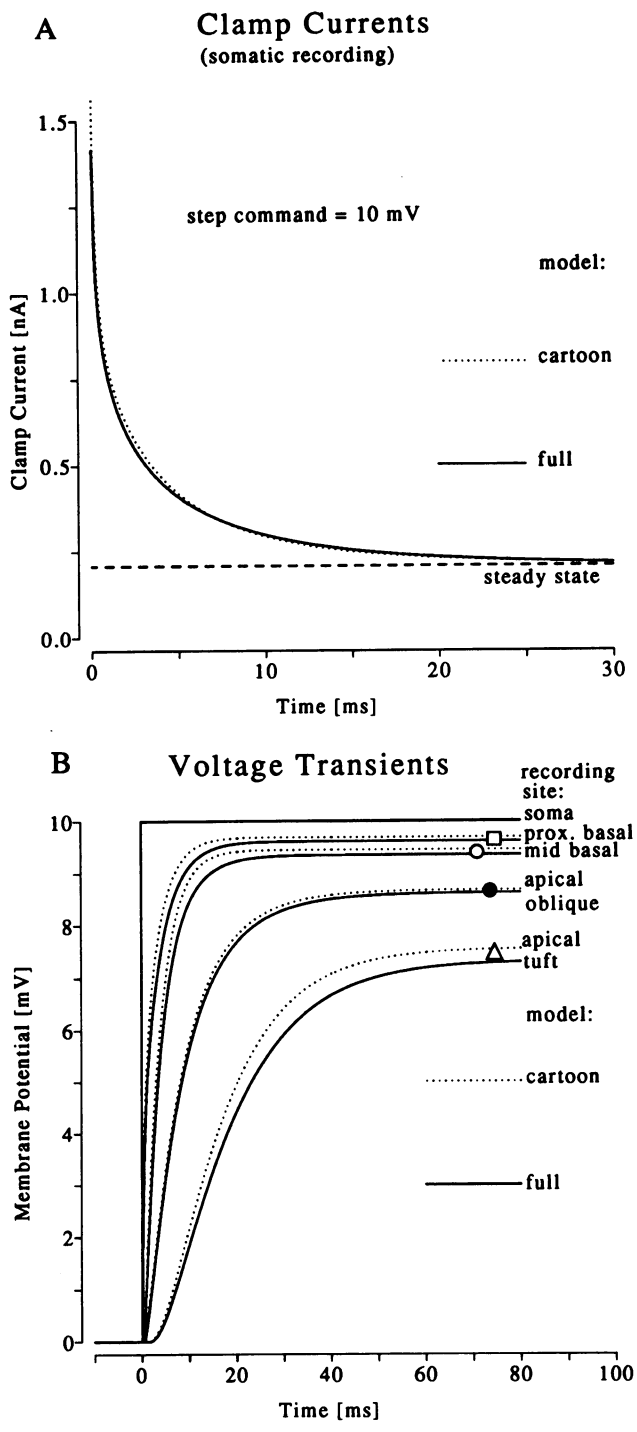


FIGURE 11 CA1 pyramidal cell, perfect voltage clamp, Case II: comparison of full model and cartoon responses to a 10-mV somatic voltage step command. (*A*) Clamp current recorded at soma. Notice the slow charge redistribution. (*B*) Local voltage responses at selected dendritic sites (see Table 3 for precise locations). Notice that the clamp is poor, both in terms of the speed of response, and the steady-state levels attained, particularly in the case of the apical tuft site.

rent. The dendritic cable alone is capable of producing a more than 10-fold slowing in the case of the oblique input in all three models. Series resistances of 100 MΩ can produce a further approximate doubling of the rise times. With a series resistance of only 2 MΩ, the default model proximal input has its $t_{2080}$ slowed by a factor of 1.55, to 0.17 ms, but the oblique input has its $t_{2080}$ slowed to 2.1 ms, by a factor of nearly 20. With a series resistance of 50 MΩ, the oblique input's $t_{2080}$ is 3.2 ms. Again, changes in $R_m$ have little effect on the proximal input. With small series resistances, changes in $R_m$ also have little effect on the oblique input. Decreasing $R_m$ reduces the oblique rise times and, perhaps counterintuitively, the proximal to midoblique separation of rise times (despite the increase in the electrotonic distance of the input from the soma). The reduction is more severe when $R_{ser}$ is large. Decreasing $R_i$ reduces the proximal to midoblique separation but accentuates the series resistance effects (as with the peak currents).

It is interesting to compare the rise times above with some of those reported experimentally for the clamp currents of the AMPA components of Schaeffer collateral inputs: e.g., around 1–4 ms (Ref. 17), $t_{1090}$ values measured, which tend to be about 50% longer than $t_{2080}$ values, $R_{ser}$ around 7 MΩ) and around 4.8 ms (Ref. 43, pipette resistances 3–8 MΩ, $R_{ser}$ possibly around three times as high, e.g., see Ref. 41).

Fig. 10 *D* shows the effective decay time constants ($\tau_{eff}$ values) of the clamp currents, when a single exponential was fitted (using a simplex algorithm) between $t_{peak}$ + 0.7 and $t_{peak}$ + 20 ms, where $t_{peak}$ is the time at which the peak current occurred (following Ref. 15). Although the clamp currents were actually composed of many different components with different time constants over the fit interval, in all cases the optimal single exponential fit appeared acceptable by eye, when examined with a linear current axis. Every fit S.D. (see Waveform Measures section above) was less than 0.0004. As emphasized in Paper I (Example 2) and above, the effective time constants change with the fit interval chosen, so it is important for experimenters to adopt a clearly specified convention.[3]

It can be seen from Fig. 10 *D* that $\tau_{eff}$ increases approximately linearly with low series resistances (less than about 20 MΩ), as was shown above for the effective time constants of a single cylinder + soma model. The more distal the input location, the larger the intercept at $R_{ser} = 0$. The lines for the proximal and midoblique locations run approximately parallel to begin with, then diverge at higher $R_{ser}$ values as the $\tau_{eff}$ of first the proximal, then the midoblique response begins to increase more slowly. The slopes of these lines are increased by lowering $R_i$ or raising $R_m$: both changes bring more dendritic capacitance electrically "near" to the clamp point, and exacerbate the series resistance effects (see Paper II, Influence of Electrical Parameters on Effect of $R_{ser}$ sec-

[3] The example in Paper I was for voltage transients measured in a model with a 100-nS shunt. As discussed in Paper II (under the Comparison to Voltage Recording with a Shunt section) the clamp currents with imperfect clamp are an upside-down version of the soma-recorded waveforms scaled by $g_{ser}$, where $g_{ser}$ is set equal to the voltage recording $g_{shunt}$. The same arguments therefore apply to the clamp current waveforms as apply to the somatic voltage transients.

tion). Interestingly, the proximal input's slope is more sensitive to $R_i$ and the midoblique input's slope is more sensitive to $R_m$, reflecting the progressive increase in importance of the membrane resistance in shaping slower events. Again, the proximal to midoblique separation is decreased by lowering $R_i$ or (perhaps counterintuitively) $R_m$.

With perfect clamp, the default model produced a proximal $\tau_{eff}$ of 2.53 ms, an increase by a factor of only 1.26 from the actual decay time constant of 2 ms. The midoblique input resulted in a $\tau_{eff}$ of 9.11 ms, an increase by a factor of over 4.5 due to the cable alone. With a series resistance of 50 MΩ, the midoblique input's $\tau_{eff}$ was 23.8 ms, an increase by over an order of magnitude. Some experimental values of decay time constants for comparison are: around 7.3 ms (mainly AMPA component; shortest 3.2 ms (27)), 40 ms (AMPA component (43)), and about 4–15 ms (AMPA component (17)). The discrepancies between some of these figures may well be caused by differences in fit intervals as well as by differences in experimental conditions.

It is worth re-emphasizing that, for a given $R_{ser}$, increasing $R_m$: (i) has virtually no effect on the peak current attenuations or proximal rise times, (ii) slows distal inputs' rise times, and (iii) slows effective decay time constants.

Rather than improving the clamp of transient inputs, deliberately increasing $R_m$ with channel blockers such as $Cs^+$ will actually worsen the distortions which occur (assuming a purely passive membrane).

Much of the plausible range of biological parameters is covered in Fig. 10. $C_m$ could well be higher, leading to even greater distortions. $R_i$ values higher than 200 Ωcm are possible (e.g., Refs. 4 and 5): they would lead to stronger cable but weaker series resistance effects. To be complete, a range of input kinetics and a larger range of electrical parameters and input locations should be explored for more than one cell. In addition, the results should be confirmed using compartmental models and conductance inputs into explicitly modelled spines (e.g., Refs. 5 and 15), to allow for reductions in driving force. This nonlinearity will further distort waveforms. Finally, the effects of dendritic active conductances should be investigated. The basic conclusion, however, is likely to stand: the majority of Schaeffer collateral inputs onto CA1 cells are extremely poorly clamped, and the recorded clamp currents are heavily attenuated and slowed, by up to an order of magnitude with reasonable parameter values.

### Case II: Responses to voltage command steps

Responses to a 10 mV voltage command step at the soma are shown in Fig. 11 for both the full model and the cartoon, under perfect clamp. The default electrical parameters above are used, including $g_{shunt}$ = 15 nS. The clamp currents are plotted in *A*: notice that there is significant charge redistribution occurring as late as 20 ms. As with the synaptic clamp currents above, there is good (but not perfect) agreement between the currents required by the two representations. The voltage responses at the sites specified above, excluding those on the apical trunk, are shown in Fig. 11 *B*. Again, there is reasonable agreement between the two representations, except possibly at the apical tuft. All sites are remarkably badly clamped: even the proximal basal site requires about 15 ms to approach the steady state. The apical tuft requires over 80 ms to reach a steady-state level of about 70% of the command step. As mentioned above, $C_m$ and $R_i$ values higher than those actually used are entirely plausible: clamp performance would then be even worse. A full exploration of parameter dependencies is not included, for reasons of space, but as with the subsynaptic voltage swings, voltage control is poor over a wide range of plausible electrical parameters. Naturally, any series resistance will make control even worse, since the soma voltage no longer tracks the command potential (see Paper II, Example 2).

## DISCUSSION

### Effective decay time constants

As in Paper I, it is possible to fit many transients over reasonably long intervals with a *single* exponential, despite the fact that they are in reality composed of *many* components with different time constants. The time constant of the optimum fit, termed the *effective* or apparent time constant $\tau_{eff}$, depends on the interval chosen. Fits are often better when the model has a complex geometry and generates many closely spaced time constants $\tau_n$. Experimenters are urged to inspect semi-log plots and to adopt clearly specified conventions for fit intervals and numbers of components, when attempting to measure the "time constant(s)" of clamp current waveforms.

### Cable effects and poor space clamp

The examples above demonstrate the difficulties of voltage clamping neurones with significant cable properties, as suggested by the combination of morphological and electrical parameters used here and in other studies (e.g., Refs. 4, 5, and 7). In Case I, the clamp of synaptic inputs, even fairly proximal synaptic inputs may be smoothed and attenuated before reaching the soma, and the recorded clamp currents may be strongly filtered versions of the true synaptic currents injected into the dendrites. Voltage control down the dendrites is also likely to be extremely poor, with the major part of the dendritic voltage swing (which is dominated by charge redistribution) hardly being affected by voltage clamping. If voltage-dependent conductances are present in the dendrites (e.g., Ref. 44), somatic voltage clamping may not be sufficient to prevent these being activated by synaptic inputs. In Case II, dendritic responses will be seriously delayed and attenuated versions of the command voltage imposed at the soma. This will complicate the interpretation of voltage clamp experiments on dendritic active conductances, especially those with rapid kinetics and distal locations.

## Relative efficacies: Voltage recording versus voltage clamp

Let $V_{er}$ and $i_{\text{clamp}_{er}}$ be the voltage and clamp current, respectively, recorded at $r$ in response to an input at $e$. Let $\hat{V}$ be the steady-state voltage. It is worth repeating a result discussed previously (Refs. 34 and 36, pp. 187–188): for a given input site and a given recording site, the steady-state relative efficacy $\hat{V}_{er}/\hat{V}_{rr}$ is the same as the relative efficacy of the time integrals of the corresponding transients (see above and Paper I, Appendix 3). The same relationship holds for the clamp currents. In addition, the steady-state voltage efficacy at a dendritic location ($d$) of a somatic ($s$) voltage clamp command ($\hat{V}_{sd}/\hat{V}_{ss}$) is the same as the steady-state efficacy, recording at the soma, of a dendritic input ($\hat{V}_{ds}/\hat{V}_{ss}$) because of the symmetry in the solution ($V_{sd} = V_{ds}$). Furthermore, the voltage efficacy ($V_{sd}/V_{ss}$) at a dendritic location of a *transient* somatic voltage clamp command $V_{com}(t)$ is the same as the clamp current efficacy ($i_{\text{clamp}_{ds}}/i_{\text{clamp}_{ss}}$) of a dendritic input $i_{syn}(t)$ with the same location and time course because of the reciprocity relation (see Paper II) $V_{sd} = -i_{\text{clamp}_{ds}}$ (and hence $V_{ss} = -i_{\text{clamp}_{ss}}$), when $V_{com}(t) = i_{syn}(t)$ with appropriate units.

Lower *peak* relative efficacy compared with *steady-state* relative efficacy is a feature of all passive cables. This discrepancy becomes more marked as the shunt at one end of the cable is increased and charge redistribution down the cable comes to play an increasingly important role. The limiting case, where the discrepancy between peak and steady-state efficacy is most pronounced, is voltage clamp (equivalent to an infinite shunt, as discussed in Paper II). For example, for the apical tuft input in Example 2, the steady-state efficacy is more than a factor of 10 higher than the peak current efficacy (clamped) but only a factor of 4 higher than the peak voltage efficacy (under voltage recording with a 15 nS somatic shunt).

The observation that voltage clamp attenuates peak responses more than voltage recording is important for experimenters interested in quantal analysis. If most of the noise experienced is due to spontaneous synaptic potentials (e.g., Ref. 33), then the technique which will yield the best signal-to-noise ratio will depend on the relative locations of the input of interest and the "noise" inputs. If the input of interest is very proximal (e.g., a mossy fiber input into a CA3 cell), then voltage clamp attenuates the noise (assuming it is predominantly from basal and more distal apical inputs) more than the "signal." If, however, the input of interest is relatively distal (e.g., a distal Schaeffer collateral input into a CA1 cell), the signal might be attenuated by voltage clamp more seriously than much of the noise (assuming this came from more proximal inputs), and voltage recording (with as small a shunt as possible) might well prove superior. If a particular connection between two neurones is subserved by a number of electrotonically dispersed synapses, differential cable filtering of the quantal currents will be stronger under voltage clamp than voltage recording. If the synapses all inject the same input current, the amplitude histogram peaks will therefore be more "smeared" with voltage clamp than with voltage recording.

## Imperfect voltage clamp

### *General points*

When synaptic inputs are fast and close to the soma, and *the access resistance is high relative to the effective capacitance of the cell* (e.g., above about 5–10 MΩ for a typical CA1 or CA3 cell (see Example 2 and Ref. 15)), the clamp currents may be badly distorted relative to those recorded with perfect clamp. Moreover, voltage control at the impalement/patch site itself may be inadequate (see Paper II, Example 2). With smaller cells (e.g., Ref. 12), one can "get away with" higher series resistances.

These findings should be a serious cause of concern to experimenters who use sharp microelectrodes to perform single electrode voltage clamp: typically these have resistances of between 10 and 50 MΩ. The same caution should be applied to the newer techniques of whole cell recording from neurones in slices, using the "blind" method (e.g., $R_{ser}$ values 10–20 MΩ (41, 45) or 10–30 MΩ (18)) or the perforated patch method (e.g., Ref. 32: $R_{ser}$ around 40–50 MΩ). The series resistances obtained with these methods are often higher than those possible with whole cell patching onto "cleaned" cells (e.g., Ref. 38). Even with the cleaning method there is no cause for complacency: incomplete patch rupture and blocking of pipettes are frequent problems and series resistances as high as 10 MΩ are not uncommon (e.g., $R_{ser}$ 5–10 MΩ (46); $R_{ser}$ 8–10 MΩ (11); $R_{ser}$ 2.5–10 MΩ (15)). With large cells such as CA3 pyramids, series resistances as low as 2 MΩ may still cause appreciable distortions of clamp currents (Refs. 5 (Chapter 6) and 15).

### *Problems with series resistance compensation*

Most clamp amplifiers have a series resistance compensation facility, but only partial compensation, usually $\leq 75\%$ (e.g., Ref. 46), is possible without introducing oscillations (e.g., Refs. 25 and 26). In order to perform series resistance compensation, it is first necessary to have accurately compensated the electrode capacitance (e.g., Ref. 25). As is the case with voltage recording ("current clamp"), it is hard to perform capacitance compensation when: (i) the electrode capacitance is distributed, for example when the electrode is deeply immersed in fluid (e.g., Ref. 47 (Chapter 3)), or (ii) the cell being recorded from has fast charge redistribution time constants blending into the electrode time constant(s), and there is no clear "break-point" between the electrode response and the cell response (e.g., Refs. 5 (Chapter 3) and 48).

In practice, performing capacitance compensation just prior to impalement or patch rupture is probably simpler than using the phase-sensitive method (48, 49): serious errors are unlikely to be introduced by the relatively small movements

associated with impalement or patch rupture. Further problems are caused when electrodes display additional noncapacitative artifacts (e.g., Refs. 5 (Chapter 3), 47, 50), although some amplifiers have additional facilities for compensating these (e.g., the $C_p$ setting of the C-slow dial on the EPC-7).

Contrary to previous results (3), there is often no easy way to separate soma charging currents from cable charging currents. However, series resistance compensation can still be performed (depending on the amplifier) by sharpening up the clamp current resulting from a voltage step command, sodium currents or fast post-synaptic currents, until the point at which oscillations just fail to occur. There is a danger, however, of "over-sharpening" caused by undetected "ringing." Better methods might be to estimate the series resistance first from the initial height of the unfiltered clamp current transient in response to a voltage step, or by the "no jump" transient balancing method described above for the EPC-7. In the latter case, the G-series dial should be set to the correct $g_{ser}$ (which may be hard if there is substantial noise or overfiltering), the C-slow dial should be turned right down to avoid miscompensating the soma capacitance, and the %COMPensation dial should be turned up until just before ringing occurs.

Since, in practical situations there will always be some residual series resistance, the results presented in the two examples above will always apply to some degree. The problems will be compounded if the series resistance is changing over time. For these reasons, rather than compensating series resistance, it may be better to *monitor* then *model* it: this issue needs to be explored more carefully.

Series resistance can also be estimated by performing bridge balance in current clamp mode. This latter technique, however, also suffers from the "no break-point" problem. More accurate but time-consuming measurements of $R_{ser}$ could also be performed under current clamp using the phase-sensitive technique (48).

### *Problems with switch clamp*

At first sight, the use of discontinuous voltage clamp (e.g., Ref. 50) might offer a way of by-passing series resistance altogether. However, as discussed by Wilson and Park (48), switch clamp in a cell with dendritic cables suffers from the no break-point problem afflicting the continuous methods (see above). To quote them:

*"The use of switching amplifiers. . .is therefore not a panacea for the problems of amplifier alignment in intracellular recording."*

The optimal switching rate cannot be determined intracellularly in a nonisopotential cell, because there is no roughly "flat portion" of the cell's voltage response (and therefore of the headstage waveform) after the electrode artifact. Nor can it be determined extracellularly, because of the following.

(i) Series resistances (and hence electrode time constants) are often 2–6-fold higher than the original pipette resistances when whole-cell recording with the "blind" (e.g., Ref. 41), standard whole cell or perforated patch methods (51);

(ii) $R_{ser}$ may be unstable over time;

(iii) what counts is the electrode artifact relative to the cell's response: it is "safe" to sample the membrane potential once the artifact has fallen to less than 1%, say, of the cell's response; and

(iv) there is a "nonsumming interaction" between the electrode and the cell: for a given $R_{ser}$, the duration of the intracellular artifact is longer than that of the extracellular artifact (Ref. 5 (Chapter 3)). This is analogous to the nonsumming interaction between different components of the cell when $R_{ser} > 0$, discussed in Paper II (Example 2).

See the Appendix for a possible (and untested) ad hoc way out of this dilemma.

Of course, switch clamp can do nothing to alleviate cable effects. However, with somatic inputs, low series resistances (a few MΩ) and careful capacitance compensation, it does seem possible to record fast synaptic currents (e.g., Ref. 9). Even so, there can be significant voltage escape at the soma (e.g., Ref. 9 (Fig. 3)), analogous to that which would occur with uncompensated series resistance.

A more thorough theoretical and practical exploration of switch clamp in neurones with dendrites is required.

### *Combined effects of dendritic cables and series resistance*

The results above suggest that the filtering effects of dendritic cables and series resistance compound one another in a less than additive way for peak clamp currents, and in a roughly additive way for rise times and apparent decay time constants (depending on the input time constants). Both effects are worse for faster inputs. Decreasing $R_i$ reduces cable effects. Increasing $R_m$ hardly changes the cable effects. Both manipulations worsen the smoothing caused by any series resistance, by improving charge transfer between the clamp amplifier and dendritic membrane capacitance. The preliminary "realistic" simulations above of Schaeffer collateral inputs into a CA1 cell (Example 2) demonstrate that with plausible combinations of parameters, all current waveform measures can be distorted by up to an order of magnitude.

To assess quantitatively cable and series resistance effects on recorded clamp currents, it will be necessary to make *fairly specific models* of the particular experimental system of interest, exploring the likely ranges of current kinetics, morphologies, electrical parameters, input locations, and series resistances (e.g., see Refs. 5 and 15). Using model cells with the inappropriate shapes or sizes, or incorrect electrical or input parameters could lead to misleading conclusions, particularly where those conclusions are optimistic, i.e., "the clamp works well enough." (For example, with reference to the clamp currents from mossy fiber inputs onto CA3 pyramidal cells, contrast the conclusions of Johnston and Brown (7) with those of Jonas et al. (15). The first of these two studies assumed slower synaptic inputs than the second and concluded that the clamp currents were probably not smoothed significantly. In the latter study, in the worst plausible cases, significant distortions could occur.)

### Overview

The two examples above illustrate a number of important practical problems concerning the experimental procedure of voltage clamping neurones with extensive dendritic trees. It is hoped that the relative ineffectiveness of voltage clamp demonstrated for the CA1 pyramidal cell model will provoke more thorough modelling studies by other investigators and more caution by experimenters in the interpretation of their results.

## SUMMARY AND CONCLUSIONS

1) It is possible to approximate the decay phases of noisy synaptic clamp currents with single exponentials over intervals when they are in reality composed of many exponential components. More complex neuronal geometries, which produce more closely spaced time constants, allow better fits. Semi-log plots should be used to inspect fits. The effective time constant $\tau_{eff}$ varies with the fit interval, so it is important to specify clearly the convention being adopted.

2) Synaptic clamp current waveform parameters depend on distance from the soma $z$, series resistance $R_{ser}$, and the time course of the synaptic current. Peak currents decrease with increasing $z$ and $R_{ser}$. The effects are stronger for faster inputs. Rise times and effective decay time constants increase with $z$, $R_{ser}$, and $\tau_{sy}$, the decay time constant of the synaptic current. The $\tau_{eff}$ values increase almost linearly with both $R_{ser}$ and $\tau_{sy}$. The rates of increase of all measures slow down near dendritic tips and with high enough series resistances.

3) Many of Jackson's approximations (3) break down (as noted by that author) if the ratio of the dendritic (infinitely extended) to somatic input conductance (without a shunt), $\rho_\infty$, is high. This is demonstrated for an example with $\rho_\infty$ of the order of 50, a plausible value for many pyramidal cells. When a voltage step is applied, soma and cable charging currents *cannot* easily be separated for such models.

4) "Subtractive" capacitance compensation techniques may seriously overestimate the true soma capacitance if extremely fast time bases (>100 kHz sampling) are not used. This can lead to other modelling errors. In such cases it may be better to perform series resistance compensation without soma capacitance compensation and to make use of the imperfect clamp solutions (or compartmental models) to fit the experimental data.

5) In a CA1 pyramidal cell model with biologically plausible electrical parameters, imposing perfect somatic voltage clamp hardly changes the peak voltage swings at synaptic input sites. The transients are insensitive to changes in specific membrane resistivity $R_m$, except at late times.

6) Under perfect clamp, synaptic clamp currents are much briefer than the corresponding synaptic potentials under voltage recording, and show more rapid fall-off in peak relative efficacy as the input site is moved away from the clamp point. Time integral relative efficacies for both voltage clamp and voltage recording are the same as the corresponding steady-state relative efficacies. With the electrical parameters used, dendritic trees based on the morphologies of real pyramidal cells can cause significant attenuation and smoothing of synaptic inputs. Again, the early parts of the transients are insensitive to $R_m$.

7) The effects of series resistance and dendritic cables compound one another, less than additively for peak currents, and roughly additively for rise times and effective decay time constants. Plausible combinations of parameters can lead to attenuation and smoothing of the clamp currents from Schaeffer collateral inputs into a CA1 cell model by up to an order of magnitude.

8) With plausible parameters, dendritic voltages resulting from a somatic voltage command step can show significant delays (15–80 ms) before reaching steady state.

9) The space clamp and voltage clamp problems outlined above are unlikely to be solved by the application of switch clamp: fundamental limitations are imposed by the electrical geometry of the cell being clamped and the properties of the electrode used.

10) The example models presented here are intended to illustrate the analytical solutions of the previous two papers, to alarm experimenters attempting to voltage clamp neurones with extensive dendritic trees, and to encourage more detailed modelling of each experimental situation.

## APPENDIX: OPTIMAL SWITCH CLAMP RATES FOR NEURONES

Problems arise when attempting to determine the optimal switching rate for discontinuous voltage clamp of neurones with nonisopotential dendrites. Suppose all the cells of a given class have similar voltage responses to brief current pulses (e.g., of 10-$\mu$s duration). A new electrode's extracellular artifact, with optimal capacitance compensation, following the pulse could be compared to a "typical" cell's response (with its own electrode control subtracted). The time $t_1$ taken for the new electrode's artifact to fall to 1% of the cell's response could be measured. There is a further complication: the response of the combined electrode-cell system is greater than the sum of the responses of electrode and cell alone (Ref. 5, Chapter 3). The presence of the cell slows the capacitative artifact of the electrode by a factor of about 3, since it is no longer discharging directly to earth. (The exact factor will depend on the electrode, the cell, and the criterion adopted for the "end" of the artifact.) The effective artifact will therefore have a duration of about $3t_1$. With a 33% duty cycle, this gives a sample interval of $\frac{1}{2} \times 3t_1$, i.e., a "safe" switch rate of $0.22/t_1$. If the series resistance and hence electrode time constant increase by a factor of $F_R$ following establishment of the recording from the cell, then the "safe" switch rate is slowed to roughly $0.22/F_R t_1$. Voltage transients much faster than this will not be adequately clamped, and the clamp currents will be slower than the real currents. Note that the duration of the original current pulse tested should be similar to the duration of the current injection phase of the switch cycle. Approximate series resistance should be monitored periodically by one of the methods described above, and adjustments to the switch rate should be made accordingly.

I would like to thank Nelson Spruston, Ken Stratford, Mike Häusser, Greg Stuart, Peter Jonas, and Bert Sakmann for helpful discussions and criticisms, and Julian Jack, Alan Larkman, and Jonathan Evans for indispensable support and advice. I am grateful to the Wellcome Trust for financial support (see Paper I (1)).

## REFERENCES

1. Major, G., J. D. Evans, and J. J. B. Jack. 1993. Solutions for transients in arbitrarily branching cables: I. Voltage recording with a somatic shunt. *Biophys J.*, 65:423–449.
2. Major, G., J. D. Evans, and J. J. B. Jack. 1993. Solutions for transients

in arbitrarily branching cables: II. Voltage clamp theory. *Biophys J.*, 65:450–468.

3. Jackson, M. B. 1992. Cable analysis with the whole-cell patch clamp. Theory and experiment. *Biophys. J.* 61:756–766.
4. Stratford, K. J., A. J. R. Mason, A. U. Larkman, G. Major, and J. J. B. Jack. 1989. The modelling of pyramidal neurones in the visual cortex. *In* The Computing Neurone. R. Durbin, C. Miall, and G. Mitchison, editors. Addison-Wesley, Reading, UK. 296–321.
5. Major, G. 1992. The physiology, morphology and modelling of cortical pyramidal neurones. D.Phil. thesis. Laboratory of Physiology, Oxford University. 275 pp.
6. Rall, W., and I. Segev 1985. Space-clamp problems when voltage clamping branched neurons with intracellular microelectrodes. *In* Voltage and Patch Clamping with Microelectrodes. T. G. Smith Jr., H. Lecar, S. J. Redman, and P. Gage, editors. American Physiological Society, Bethesda, MD. 191–215.
7. Johnston, D., and T. H. Brown. 1983. Interpretation of voltage-clamp measurements in hippocampal neurons. *J. Neurophysiol.* 50:464–486.
8. Spruston, N., D. B. Jaffe, S. H. Williams, and D. Johnston. 1993. Voltage and space clamp errors associated with the measurement of electrotonically remote synaptic events. *J. Neurophysiol.* In press.
9. Finkel, A. S., and S. J. Redman. 1983. The synaptic current evoked in cat spinal motoneurones by impulses in single group 1a axons. *J. Physiol.* 342:615–632.
10. Edwards, F. A., A. Konnerth, and B. Sakmann, with an appendix by C. Busch. 1990. Quantal analysis of inhibitory synaptic transmission in the dentate gyrus of rat hippocampal slices: a patch-clamp study. *J. Physiol.* 430:213–249.
11. Keller, B. U., A. Konnerth, and Y. Yaari. 1991. Patch clamp analysis of excitatory synaptic currents in granule cells of rat hippocampus. *J. Physiol.* 435:275–293.
12. Silver, R. A., S. F. Traynelis, and S. G. Cull-Candy. 1992. Rapid-time-course miniature and evoked excitatory currents at cerebellar synapses in situ. *Nature*. 355:163–166.
13. Colquhoun, D., P. Jonas, and B. Sakmann. 1992. Action of brief pulses of glutamate on AMPA/kainate receptors in patches from different neurones of rat hippocampal slices. *J. Physiol.* 458:261–287.
14. Stern, P., F. A. Edwards, and B. Sakmann. 1992. Fast and slow components of unitary EPSCs on stellate cells elicited by focal stimulation in slices of rat visual cortex. *J. Physiol.* 449:247–278.
15. Jonas, P., G. Major, and B. Sakmann. 1993. Quantal analysis of unitary EPSCs at the mossy fiber synapse on CA3 pyramidal cells of rat hippocampus. *J. Physiol.* In press.
16. Nelson, P. G., R. Y. K. Pun, and G. L. Westbrook. 1986. Synaptic excitation in cultures of mouse spinal cord neurones: receptor pharmacology and behavior of synaptic currents. *J. Physiol.* 372:169–190.
17. Hestrin, S., R. A. Nicoll, D. J. Perkel, and P. Sah. 1990. Analysis of excitatory synaptic action in pyramidal cells using whole-cell recording from rat hippocampal slices. *J. Physiol.* 422:203–225.
18. McBain, C., and R. Dingledine. 1992. Dual-component miniature excitatory synaptic currents in rat hippocampal CA3 pyramidal neurones. *J. Neurophysiol.* 68:16–27.
19. Clements, J. D., and S. J. Redman. 1989. Cable properties of cat spinal motoneurons measured by combining voltage clamp, current clamp and intracellular staining. *J. Physiol.* 409:63–87.
20. Rall, W. 1969. Time constants and electrotonic length of membrane cylinders and neurons. *Biophys. J.* 9:1483–1508.
21. Press, W. H., B. P. Flannery, S. A. Teukolsky, and W. T. Vetterling. 1988. Numerical Recipes in C: The Art of Scientific Computing. Cambridge University Press, Cambridge, UK. 735 pp.
22. Larkman, A. U., G. Major, K. J. Stratford, and J. J. B. Jack. 1992. Dendritic morphology of pyramidal neurones of the visual cortex of the rat: IV. Electrical geometry. *J. Comp. Neurol.* 323:153–166.
23. Larkman, A., and A. Mason. 1990. Correlations between morphology and electrophysiology of pyramidal neurons in slices of rat visual cortex. I. Establishment of cell classes. *J. Neurosci.* 10:1407–1414.
24. Major, G., A. U. Larkman, and J. J. B. Jack. 1990. Constraining non-uniqueness in passive electrical models of cortical pyramidal neurones. *J. Physiol.* 430:23P.
25. Sigworth, F. J. 1983. Electronic design of the patch clamp. *In* Single-Channel Recording. B. Sakmann, and E. Neher, editors. Plenum Press, New York. 3–35.
26. Sigworth, F. J. 1985. EPC-7 User's Manual. List-electronic, Darmstadt, Germany. 74 pp.
27. Bekkers, J. M., G. B. Richerson, and C. F. Stevens. 1990. Origin of variability in quantal size in cultured hippocampal neurons and in hippocampal slices. *Proc. Natl. Acad. Sci. USA.* 87:5359–5362.
28. Malinow, R., and R. W. Tsien. 1990. Presynaptic enhancement shown by whole-cell recordings of long-term potentiation in hippocampal slices. *Nature* 346:177–180.
29. Randall, A. D., J. G. Schofield, and G. L. Collingridge. 1991. Patch-clamp recordings of spontaneous and evoked minimal synaptic currents from CA1 neurones of rat hippocampal slices. *J. Physiol.* 438:256P.
30. Malinow, R. 1991. Transmission between pairs of hippocampal slice neurons: quantal levels, oscillations, and LTP. *Science*. 252:722–725.
31. Manabe, T., P. Renner, and R. A. Nicoll. 1992. Postsynaptic contribution to long-term potentiation revealed by the analysis of miniature synaptic currents. *Nature*. 355:50–55.
32. Kullman, D. M., and R. A. Nicoll. 1992. Long-term potentiation is associated with increases in quantal content and quantal amplitude. *Nature*. 357:240–244.
33. Larkman A., K. Stratford and J. Jack. 1991. Quantal analysis of excitatory synaptic action and depression in hippocampal slices. *Nature*. 350:344–347.
34. Rinzel, J., and W. Rall. 1974. Transient response in a dendritic neuron model for current injected at one branch. *Biophys. J.* 14:759–790.
35. Abbott, L. F. 1992. Simple diagrammatic rules for solving dendritic cable problems. *Physica A.* 185:343–356.
36. Jack, J. J. B., D. Noble, and R. W. Tsien. 1975. Electric Current Flow in Excitable Cells. Oxford: Oxford University Press, Oxford, UK. 502 pp.
37. Shelton, D. P. 1985. Membrane resistivity estimated for the Purkinje neuron by means of a passive computer model. *Neuroscience.* 14:111–131.
38. Edwards, F. A., A. Konnerth, B. Sakmann, and T. Takahashi. 1989. A thin slice preparation for patch clamp recordings from neurones of the mammalian central nervous system. *Pflügers Arch.* 414:600–612.
39. Pongracz, F., S. Firestein, and G. M. Shepherd. 1991. Electrotonic structure of olfactory sensory neurons analyzed by intracellular and whole cell patch techniques. *J. Neurophysiol.* 65:747–758.
40. Spruston, N., and D. Johnston. 1992. Perforated patch-clamp analysis of the passive membrane properties of three classes of hippocampal neurons. *J. Neurophysiol.* 67:503–529.
41. Staley, K. J., T. S. Otis, and I. Mody. 1992. Membrane properties of dentate gyrus granule cells: comparison of sharp microelectrode and whole-cell recordings. *J. Neurophysiol.* 67:1346–58.
42. Liao, D., A. Jones, and R. Malinow. 1992. Direct measurement of quantal changes underlying long-term potentiation in CA1 hippocampus. *Neuron*. 9:1089–1097.
43. Randall, A. D., and G. L. Collingridge. 1990. Kinetic properties of NMDA and AMPA receptor-mediated EPSCs recorded from rat hippocampal slices under whole-cell voltage clamp. *J. Physiol.* 431:41P.
44. Hounsgaard, J., and J. Midtgaard. 1989. Dendrite processing in more ways than one. *Trends Neurosci.* 12:313–315.
45. Blanton, M. G., J. J. Lo Turco, and A. R. Kriegstein. 1989. Whole cell recording from neurons in slices of reptilian and mammalian cerebral cortex. *J. Neurosci. Meth.* 30:203–210.
46. Llano, I., A. Marty, C.M. Armstrong, and A. Konnerth. 1991. Synaptic- and agonist-induced excitatory currents of Purkinje cells in rat cerebellar slices. *J. Physiol.* 434:183–213.
47. Purves R. D. 1981. Microelectrode Methods for Intracellular Recording and Iontophoresis. Academic Press, London, UK. 146 pp.
48. Wilson, C. J., and M. R. Park. 1989. Capacitance compensation and bridge balance adjustment in intracellular recording from dendritic neurons. *J. Neurosci. Meth.* 27:51–75.
49. Park, M. R., H. Kita, M. R. Klee, and Y. Oomura. 1983. Bridge balance in intracellular recording; introduction of the phase-sensitive method. *J. Neurosci. Meth.* 8:105–125.
50. Finkel, A. S., and S. J. Redman. 1984. Theory and operation of a single microelectrode voltage clamp. *J. Neurosci. Meth.* 11:101–127.
51. Korn, S. J. and R. Horn. 1989. Influence of sodium-calcium exchange on calcium current rundown and the duration of calcium-dependent chloride currents in pituitary cells, studies with whole cell and perforated patch recording. *J. Gen. Physiol.* 94:789–812.